EMPIRICAL GRAVITIES AND TEMPERATURES FOR

DA TYPE WHITE DWARFS

by

Santiago Tapia Perez

A Dissertation Submitted to the Faculty of the

DEPARTMENT OF ASTRONOMY

In Partial Fulfillment of the Requirements
For the Degree of

DOCTOR OF PHILOSOPHY

In the Graduate College

THE UNIVERSITY OF ARIZONA

1 9 7 8

7823776

TAPIA PEREZ, SANTIAGO
  EMPIRICAL GRAVITIES AND TEMPERATURES FOR DA
  TYPE WHITE DWARFS.

THE UNIVERSITY OF ARIZONA, PH.D., 1978

EMPIRICAL GRAVITIES AND TEMPERATURES FOR

DA TYPE WHITE DWARFS

by

Santiago Tapia Perez

_____

A Dissertation Submitted to the Faculty of the

DEPARTMENT OF ASTRONOMY

In Partial Fulfillment of the Requirements
For the Degree of

DOCTOR OF PHILOSOPHY

In the Graduate College

THE UNIVERSITY OF ARIZONA

1 9 7 8

THE UNIVERSITY OF ARIZONA

GRADUATE COLLEGE

I hereby recommend that this dissertation prepared under my
direction by ___Santiago Tapia Perez_____
entitled ___Empirical Gravities and Temperatures of_____

___DA Type White Dwarfs,_____

be accepted as fulfilling the dissertation requirement for the

degree of ___Doctor of Philosophy._____

_P. A. Strittmatter_____   _4-14-78_
Dissertation Director   **Date**

As members of the Final Examination Committee, we certify
that we have read this dissertation and agree that it may be
presented for final defense.

David L. Crawford	_4-14-78_
Neville J. Woolf	_4-14-78_
J. R. P. Angel	_4-17-78_
_____	_____
_____	_____
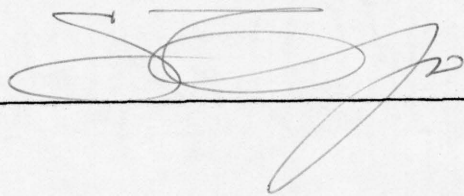
Final approval and acceptance of this dissertation is contingent
on the candidate's adequate performance and defense thereof at the
final oral examination.

STATEMENT BY AUTHOR

This dissertation has been submitted in partial fulfillment of requirements for an advanced degree at The University of Arizona and is deposited in the University Library to be made available to borrowers under rules of the Library.

Brief quotations from this dissertation are allowable without special permission, provided that accurate acknowledgment of source is made. Requests for permission for extended quotation from or reproduction of this manuscript in whole or in part may be granted by the head of the major department or the Dean of the Graduate College when in his judgment the proposed use of the material is in the interests of scholarship. In all other instances, however, permission must be obtained from the author.

SIGNED: _____

ACKNOWLEDGMENTS

The investigation reported here was made possible and pleasant by the help and suggestions of the faculty and staff of Steward Observatory. Sincere thanks are expressed to:

R. McCallister and the mountain personnel for their tireless concern with the equipment and the telescope during observing runs;

M. Reed for advice on the electronic components. His help made sailing through rough waters easy and elegant, even if it took some tacking into the wind;

T. Sargent for coming to the rescue of several observing runs with his expert support. Each occasion was also a demonstration that computers do indeed obey him;

P. A. Strittmatter and R. J. Weymann for their marvelous impersonations of Ernie and Bert (respectively), and for the numerous opportunities to do research that they give the students of astronomy at The University of Arizona;

G. V. Coyne, T. Gehrels, and K. Serkowski for support and encouragement during the last three years.

It is also a pleasure to acknowledge the stimulation and encouragement I have been afforded during this work by the many discussions with P. A. Strittmatter. Especially appreciated are his frequent departures from a busy administrative schedule to discuss research, and his cheerful skepticism.

During the early part of this work, the author benefited from an AURA, Inc. Fellowship. Later, partial support was provided by the National Science Foundation.

TABLE OF CONTENTS

TABLE OF CONTENTS--<u>Continued</u>

LIST OF TABLES

LIST OF TABLES--<u>Continued</u>

LIST OF ILLUSTRATIONS

ABSTRACT

A sample of 46 DA white dwarfs were observed with a four band photometric system designed to improve the determination of surface gravities and effective temperatures of this class of stars. The spectral sensitivity of the photometric bands was derived by independent measurements of the transmission optics and filters, and the relative response of the detector. The spectral sensitivity of each band was convolved with the energy distribution of DA white dwarfs model atmospheres to compute synthetic color indices. The synthetic and observed colors were matched on the plane defined by two reddening-free indices in order to derive gravities and temperatures. The results indicate that a majority of DA white dwarfs are characterized by a narrow range of gravities around $\log(g) = 8$. Combination of the effective temperatures with bolometric magnitudes for a subset of stars with accurate trigonometric parallax lends support to the existence of two sequences of degenerate dwarfs on the H-R diagram.

CHAPTER 1

INTRODUCTION

Consistent interpretation of the energy distribution emitted by stellar atmospheres indicates that the observed spectral features can be parameterized in terms of the chemical composition, the surface gravity, and the effective temperature. Observational evidence restricts the range of effective temperature to $3.3 \leq \log(T_{eff}) \leq 5$, and the range of chemical compositions to $0.001 \leq Z/H \leq 0.04$, where Z/H is the mass ratio of elements heavier than helium to hydrogen. Hydrostatic equilibrium, between the gravitational force and the pressure force of a perfect gas, restricts the gravity to $\log(g) \leq 5$ for the majority of the stars. For a highly reduced group of stars the gravitational force is balanced by the pressure force provided by electron degeneracy. In this equilibrium regime the surface gravity appears to be restricted to $7.5 \leq \log(g) \leq 8.5$. The low gravity group—characterized as the ordinary stars— includes subdwarf, main sequence, giant, and supergiant stars. Only degenerate dwarfs populate the large gravity

1

group. Due mainly to this large difference in surface
gravity, there is only a remote resemblance between
the spectra of degenerate dwarfs and ordinary stars. As
was recognized earlier in the study of these stars, such
differences require different observational techniques
in order to isolate the effects of a given atmospheric
parameter. Very satisfactory results have been obtained
with photometric systems planned to study ordinary stars.
However, consideration of a system for special applica-
tion to degenerate dwarfs has been long delayed. The
need for an improved photometric system for degenerate
dwarfs was first suggested by Luyten (1963). Graham
(1972), and more recently Bessell and Wickramasinghe
(1978), have documented the observational problems with
the Stromgren system due to the broad spectral features
of the DA white dwarfs.

The purpose of this work is to describe the re-
sults of observations with a photometric system designed
to optimise the derivation of gravity and temperature of
a particular class of degenerate dwarfs.

DA White Dwarfs

In terms of the original spectral classification
of degenerate dwarfs (Luyten 1945), the most prominent
type is formed by DA white dwarfs. According to Liebert
(1976), in a catalogue of 424 degenerate dwarfs with

3

absolute magnitude brighter than 11.75 mag, 75 percent of the entries have DA identification. The rest of the catalogue is formed essentially by DB and DO white dwarfs. In principle all these stars are available for observational studies; however, the intrinsic low luminosity of the degenerate dwarfs seriously reduces the number from which accurate observations can be obtained after moderate efforts. Only from the relatively large number of DA white dwarfs it is possible to draw a sample with statistical significance.

Aside from their larger population, these stars are characterized by a simple spectrum which leaves a very small margin for misidentification. In the optical region there are only features due to hydrogen opacity. The Balmer series is typically present only up to about H_8, and the lines exhibit strong effects of pressure broadening. The combination of these two characteristics results in a distinctive spectrum reflecting the high surface gravity of the degenerate stars.

Although the pressure and the gravity in a stellar atmosphere are connected by a complicated relationship, to a first approximation both the gas and the electron pressure are proportional to the square root of the gravity (Unsold 1955). Accordingly, degenerate dwarfs, with 10^4 times the gravity of main sequence stars,

will have 10^2 times more atmospheric pressure or about 10^5 dyn cm^{-2} in absolute values. In such dense atmospheres, perturbation of the atomic energy levels by nearby particles becomes very important. If the disturbing particles are charged, i.e., electrons and/or ions, the electric field of interaction is proportional to the inverse square of the distance between the neutral atom and the charged particle. This type of perturbation of the energy levels is known as statistical Stark effect. Encounters between neutral atoms are less important because the interaction is achieved through the dipole field, which is proportional to the inverse cube of the distance.

If the binding energy of an atomic electron is smaller than the perturbation caused by the surrounding ions, the energy level is destroyed, producing what is known as pre-ionization. This effect plays a significant part in the premature ending of the Balmer series observed in DA white dwarfs. An example of this effect is observed in the energy distribution of EG 42 (= HZ 14), presented in Figure 1.

The energy levels that are not destroyed are shifted. Due to the small mean free path in the dense atmospheric plasma of degenerate dwarfs, the atoms are almost permanently embedded in static fields. Therefore,

Figure 1.   The u, s, β, and y photometric bands. -- Wavelength in the abscissa, and normalized flux density for the energy distribution or normalized responsivity for the spectral bands and the photometer in the ordinate. The passbands, with dashed lines, are presented as fraction of the photomultiplier responsivity; this one marked with dots. The u and the y bands are defined by the respective Stromgren filters. The two new bands are s and β. For reference, the energy distribution of the DA white dwarf EG 42 is presented with a solid line. In the rest of this work, reference is made to the white dwarfs in terms of the EG numbers. Cross references can be found in the catalog prepared by McCook and Sion (1977).
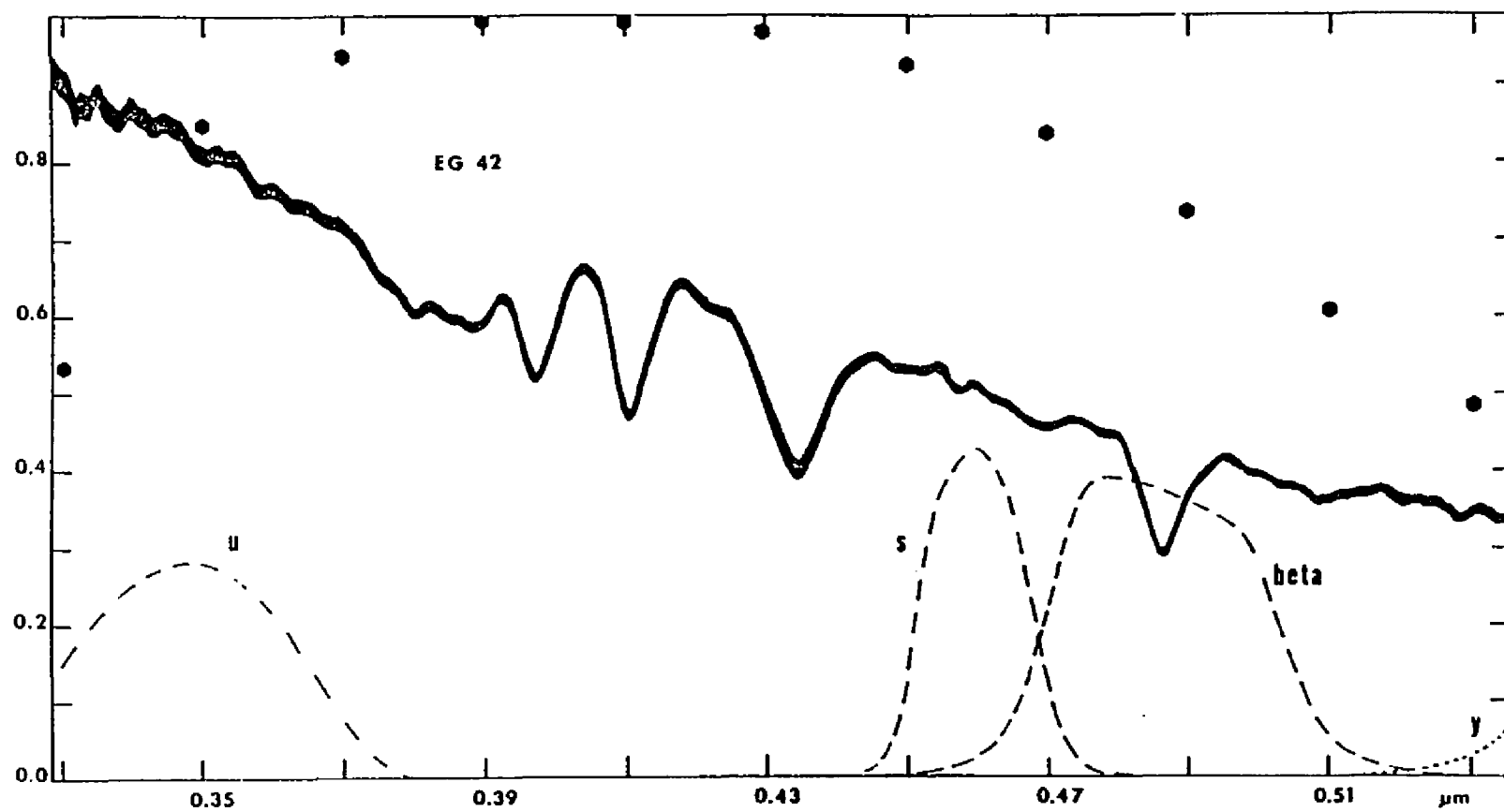
Figure 1. The u, s, β, and y photometric bands.

the energy levels remain shifted longer than the time needed for an electronic transition. In this case, in order to compute the profile of the lines observed from the transitions in a collection of atoms, it is only necessary to calculate the probability that an atom finds itself in a static field of a given intensity. This approach, developed by Holtsmark (1931), is known as the statistical Stark broadening. It can be shown that this type of broadening is proportional to the 2/3 power of the pressure. Consequently, white dwarfs with about 10^2 times the pressure of main sequence stars show about 20 times stronger Stark broadening. Figure 2 illustrates the Stark broadening in the absorption lines of the DA white dwarf EG 99 (= G14-58).

According to the statistical Stark broadening, the line opacity in the wings (i.e., for $|\Delta\lambda| > 30$ Å) decreases as $|\Delta\lambda|^{-5/2}$. Overlapping of the wings is reached between H_γ and H_δ, and merging of the lines is observed at about H_8. Pre-ionization and line merging cause the apparent absence of the higher members of the Balmer series observed in DA white dwarfs.

As in the main sequence stars the Balmer lines in degenerate dwarfs are relatively weak at high and low atmospheric temperatures, reaching maximum strength in between. The maximum is caused by the onset of H^-

Figure 2. Overlapping of H_β and the Stromgren b band. -- Abscissa and ordinate as in Figure 1. [β]The advantages of the s band over the Stromgren b band are illustrated in relation to the energy distribution of the DA white dwarf EG 99. The spectrophotometric data for EG 42 (presented in Figure 1) and EG 99 were obtained by John W. Robertson and Peter A. Strittmatter with a 40-element Digicon system attached to the Cassegrain spectrograph at the Steward Observatory 228-cm telescope. The detector system has been described by Beaver and McIlwain (1971) and the data reductions have been outlined by Carswell et al. (1975).
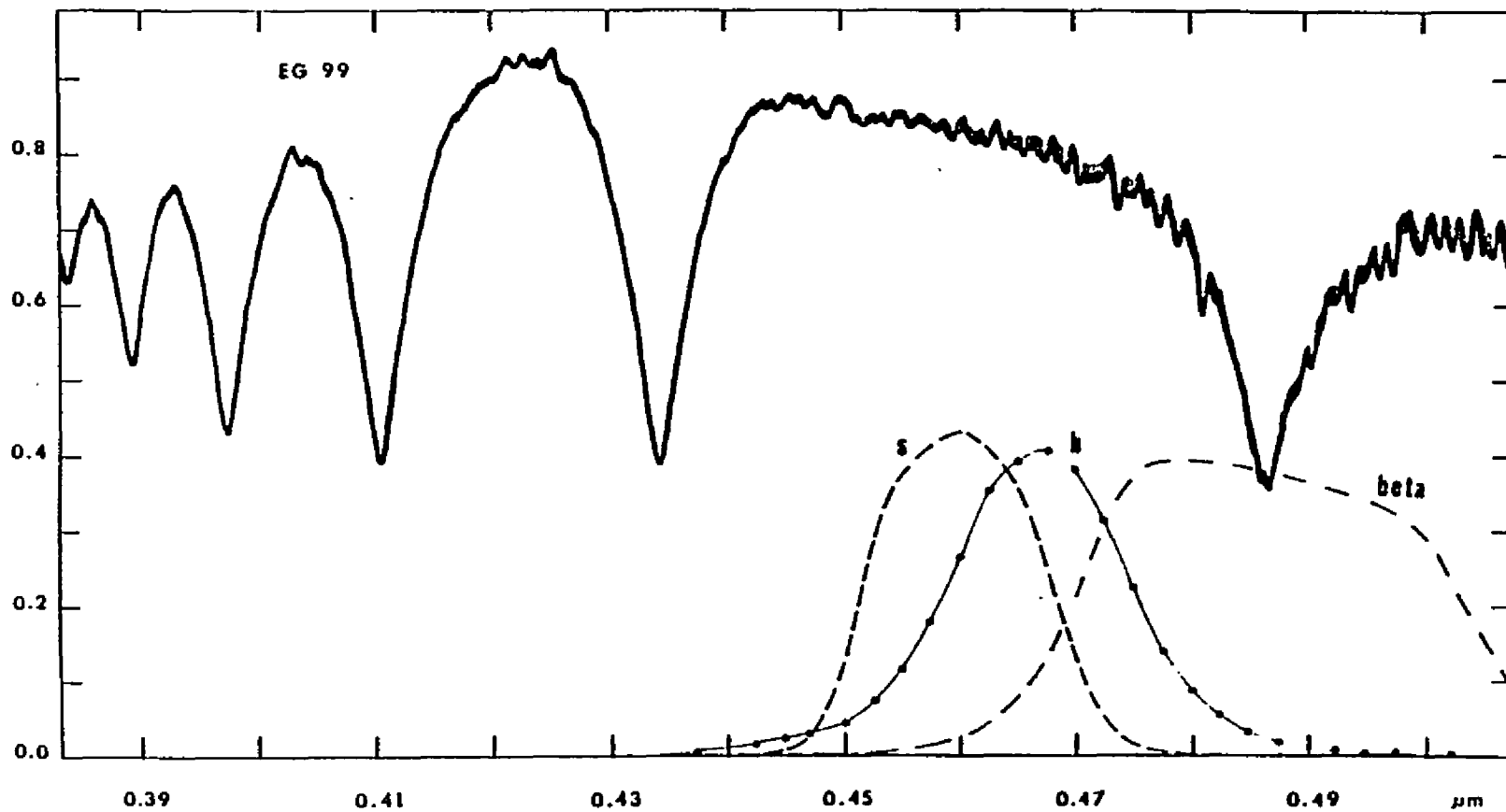
Figure 2. Overlapping of H_β and the Strömgren b band.

opacity and the strength of the gravity force. In main
sequence stars, the maximum occurs near 8500 K, However,
as documented by Weidemann (1963), the higher gravity of
DA white dwarfs shift the maximum strength to atmospheric
temperatures near 13000 K. For a large number of DA
white dwarfs, the variation of the observed equivalent
width of H_γ with respect to the (U-V) color, a fairly
good temperature indicator, has been published by Eggen
and Greenstein (1965a). Such variation is reproduced,
in general terms, by blanketed model atmospheres for high
gravities. The grid of model atmosphere published by
Wickramasinghe (1972) has been used to derive the total
width of H_β at 0.85 residual intensity as a function of
temperature and gravity, and the results are presented in
Figure 3. Dots are used to represent the data derived
from the theoretical models, with continuous lines
representing free hand interpolations.

Consequently, a photometric study of DA white
dwarfs should consider the spectroscopic characteristics
illustrated in Figures 1-3, namely: the extension of the
Balmer continuum to longer wavelengths (3850 $\overset{o}{A}$), the
overlapping of the line wings due to strong pressure
broadening, and the variation of the lines strength with
temperature.

Figure 3.   Theoretical strength of H_β in DA
           atmospheres. -- The width of H_β measured
           in Angstrom units, at 0.85 residual
           intensity, as a function of temperature
           and gravity. These results were ob-
           tained with the high gravity, blanketed
           model atmospheres published by
           Wickramasinghe (1972).
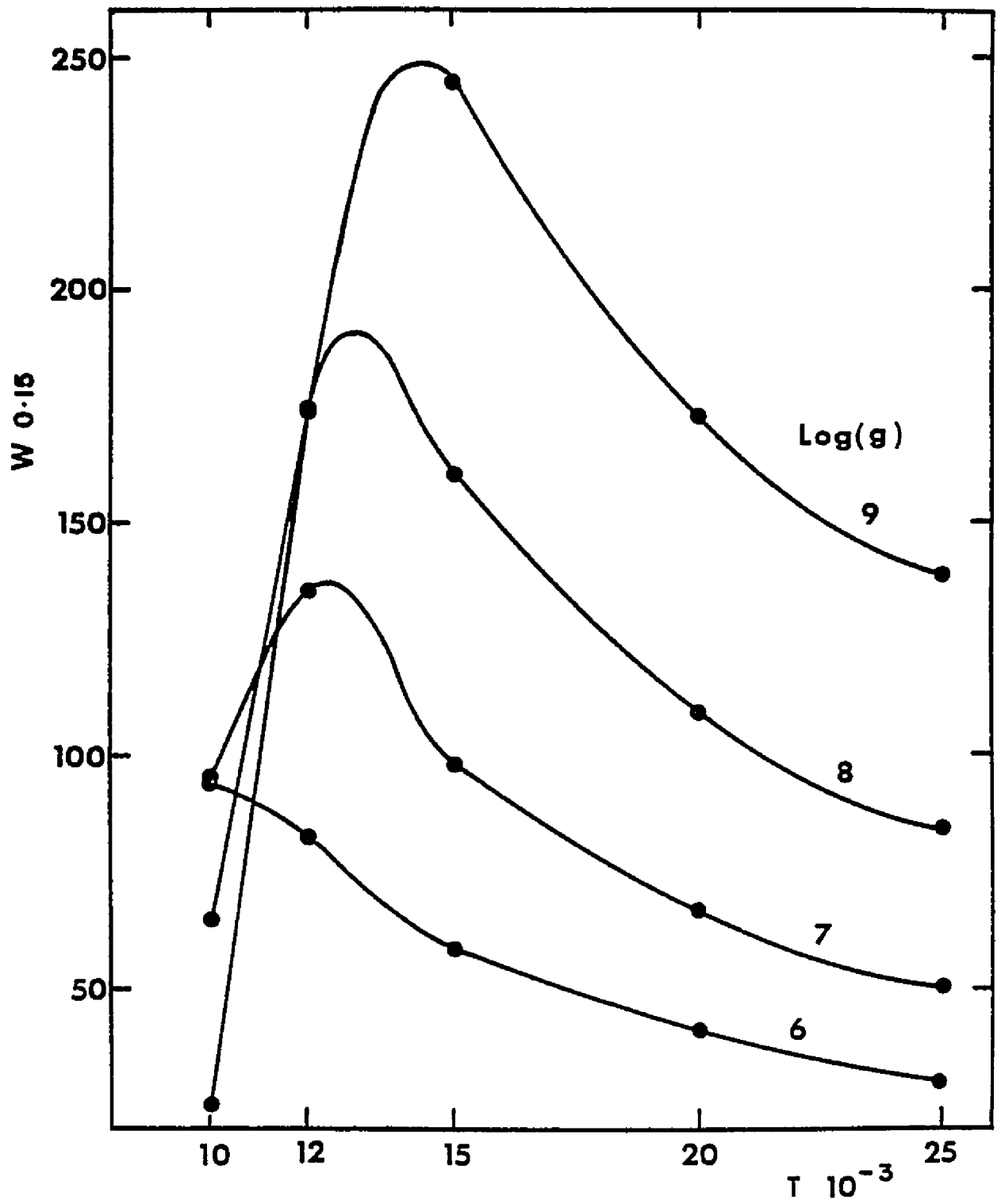
Figure 3. Theoretical strength of H_β in DA atmospheres.

Suitable Photometric Bands

An analysis of several attempts to derive atmospheric parameters of degenerate dwarfs using the Johnson broad-band and the Stromgren intermediate-band system led Wickramasinghe and Strittmatter (1972) to suggest photometric bands in accordance with the spectral characteristics of DA white dwarfs. The bands were chosen to provide both a temperature and a gravity indicator.

From the study of early type main sequence stars it is well known that, at high temperatures when the effects of H^- opacity are insignificant, the ratio of intensities between the Balmer and Paschen continua provides a good index of temperature. In line with these ideas, Wickramasinghe and Strittmatter (1972) suggested to observe the Balmer continuum with one band, and the Paschen continuum with two bands located between the first three members of the Balmer series. In order to measure the flux shortward of 3800 $\overset{o}{A}$ and between H_α and H_β the Stromgren u and y bands were retained. A new band, centered at 4600 $\overset{o}{A}$ and half width of about 200 $\overset{o}{A}$, was proposed to observe the Paschen continuum between H_γ and H_β. In Figure 1, this band (herein referred to as the s band) is illustrated in relation to the u and y bands. As indicated in Figure 2, the Stromgren b band is contaminated by the blue wing of H_β; therefore, a

measure of the continuum in the spectral region of the
b band becomes difficult to interpret.

The gravity index suggested by Wickramasinghe and
Strittmatter (1972) is based on the strength of H_β. For
this purpose they propose a photometric band centered
at 4861 $\overset{o}{A}$ with a half width of approximately 350 $\overset{o}{A}$.
A comparison of the flux measured by this band with the
flux measured by the s and y bands provides an index of
the strength of H_β, and consequently of the surface
gravity.

Approximated passbands of u, s, β, and y were
used by Wickramasinghe and Strittmatter (1972) to investi-
gate the temperature and gravity indicators derived from
the grid of model atmospheres published by Wickramasinghe
(1972). The results were encouraging because the separa-
tion of the theoretical iso-gravity and iso-temperature
curves was found to be larger than the estimated photo-
metric errors. Following these tentative results, the
four bands were implemented as described in Figures 1 and
2 in order to obtain systematic observations of DA white
dwarfs.

Background and Motivation

The internal structure and evolution of degener-
ate dwarfs can be understood, in a first approximation,
in terms of the theory developed by Fowler (1926) and

Chandrasekhar (1939). Several theoretical items, still under investigation, have been reviewed by Ostriker (1971). A controversy has developed around one such item due to the lack of observational verification. It concerns the balance of energy in degenerate dwarfs.

It is generally accepted that nuclear reactions are not possible in degenerate stars because the Coulomb barriers of the available nuclei are too high at the existent internal temperature and density. Consequently, nuclear energy is not available and only remaining sources of energy need to be considered. The original theory analyses first the case of a degenerate star at zero temperature for which only the gravitational energy Ω and the exclusion energy of the degenerate electrons U_d are available. If the velocities of the electrons are not relativistic it is possible to demonstrate that $U_d = -\Omega/2$. According to this result the star has reached an equilibrium state corresponding to half the gravitational energy, and an equal amount of energy has been used to bring all the electrons into the degenerate regime. A more common way to express this result is that degenerate electrons provide the temperature-independent pressure supporting the star against gravity. There is no dissipation of energy from stars with these characteristics; they are referred to as black dwarfs.

If the velocities of the degenerate electrons are relativistic the total energy of a black dwarf is still finite; however, such conditions are possible for the upper limit of the mass only. For a non-rotating black dwarf, Chandrasekhar (1939) found that such limit corresponds to 1.44 solar masses.

Salpeter (1961) introduced the next approximation in the energy balance for a black dwarf by considering the influence of the ions in the internal structure. To the extent that the exclusion energy of the electrons is the only form (or at least the dominant form) of internal energy in a black dwarf, ions must be forced into their lowest energy state. In such state ions are at rest in a body-centered cubic lattice. The sum of Coulomb interactions between the ionic lattice and a uniform charge of electrons provides a small but significant contribution to the total energy. According to Salpeter (1961) this contribution is also the potential energy of an inverse square law of force and can enter in the energy balance as a correction to the gravitational energy. Consequently, in this approximation $U_d = -(\Omega+V)/2$ where V is the energy due to Coulomb interactions. In this condition some gravitational energy has been transformed into Coulomb energy and the equilibrium of the star is maintained by the pressure of

degenerate electrons plus the small contribution of electrostatic interactions. The fact that the ratios V/U_d and V/Ω are much smaller than unity makes Chandrasekhar's model a good approximation up to this point.

A more realistic model is found in the degenerate dwarfs with temperature above zero: the white dwarfs. In the interior of these stars all but a very small fraction of the electrons are degenerate, ions are not degenerate, and an incipient lattice is present in the core. The main difference with black dwarfs is that ions are provided with thermal energy. Therefore, the energy balance of white dwarfs takes the form

$$2U_i + 2U_d + \Omega + V = 0 \tag{1}$$

where U_i represents the thermal energy of the ions. Because the heat capacity of the few nondegenerate electrons is negligible next to that of ions their contribution can be ignored. It can be shown that the equilibrium of a white dwarf is maintained in essentially the same way as black dwarfs. Consequently, the thermal energy of the ions amounts to $U_i = -(\Omega+V)/2$. In other words, the potential and the Coulomb energies of a white dwarf are equally divided into the exclusion energy of

degenerate electrons and the thermal energy of the ions.
This last form of energy is dissipated from the star and
part of it is observed as radiation in the optical region.
While this energy is consumed white dwarfs cool down, at
approximately constant radius, evolving to the black
dwarf stage.

It is clear now that if a star reaches the stage
of white dwarf without a lattice in the core, at some
point during the dissipation of thermal energy from the
ions Coulomb interactions became sufficiently strong to
hinder the motion of nuclei ensuing the formation of a
lattice. After that point, crystallization originates
in the core of the white dwarf and further cooling brings
a large fraction of the stellar interior into crystal-
lization.

A detailed analysis of the energy balance in a
white dwarf near the transition to black dwarf was made
by Mestel and Ruderman (1967). They considered the
effects of slight contraction with cooling and the re-
lease of small amounts of gravitational energy, the
contributions of kinetic and Coulomb energies due to
oscillations of the lattice, and the changes of heat
capacity as the lattice grows. The results indicate
that near zero temperature dissipation of thermal plus
Coulomb energy is comparable to the variation of

gravitational energy. However, the gravitational energy released by the white dwarf is almost entirely absorbed by the increase in exclusion energy of degenerate electrons.

Mestel and Ruderman (1967) also deduced that over the temperature range relevant to white dwarfs the heat capacity is dominated by Coulomb contributions from the ionic lattice. Consequently, the Dulong-Petit law $c_v \simeq 3k$, where k is the Boltzmann constant, gives a better approximation to the specific heat per ion than the value for a classical gas $c_v \simeq 3/2k$

Variations of the heat capacity due to crystallization have been investigated in terms of two different hypotheses. In the first case Mestel and Ruderman (1967) considered crystallization as the result of a continuous transition between liquid and solid at essentially constant volume. Under these conditions degenerate dwarfs maintain the same heat capacity before and after the lattice formation. For a total mass M containing ions of molecular weight μ the heat capacity can be determined from

$$C_v = 3k\frac{M}{\mu H} \qquad (2)$$

where H is the unit of atomic mass. It follows then that
the luminosity of the degenerate dwarfs is given by

$$L = -\frac{d}{dt}(3k\frac{M}{\mu H}T) \tag{3}$$

which corresponds to the rate of change of the thermal
energy of the nondegenerate ions.

Van Horn (1968) adopted the alternative case of
an abrupt change in the symmetry of the distribution of
ions during crystallization. In this case there is a
reduction in the average Coulomb interaction energy per
particle due to the transition to the solid phase. The
energy released is the latent heat of crystallization,
amounts to about kT per ion, and adds to the internal
energy. The net result is an increase in the heat
capacity with the corresponding increase of the lumi-
nosity. As derived by Van Horn (1968), the luminosity
of a partially crystallized degenerate dwarf is given by

$$L = -(1 + f) \frac{d}{dt}(3k\frac{M}{\mu H}T) \tag{4}$$

where f > 0 depends on the fraction of the mass affected
by crystallization and the molecular weight of the ions
involved.

In principle the increase in luminosity may be significant enough to allow detection of crystallization sequences in the H-R diagram. Degenerate dwarfs with ions of larger molecular weight should release more latent heat and consequently such stars may populate brighter sequences in the H-R diagram. Van Horn (1968) documented the characteristics of crystallization sequences for white dwarfs of different chemical composition. On the $\log(L)$ versus $\log(T_{eff})$ diagram crystallization sequences display a shallower slope than the lines of constant radius, a characteristic that is supported by the observational data published by Eggen and Greenstein (1965a). The existence of crystallization sequences was denied later by Weidemann (1975) with arguments based on Stromgren photometry obtained by Graham (1972).

As mentioned in the former section the b band of the Stromgren system may contain significant contamination from H_β which makes the (b-y) color a poor temperature indicator for white dwarfs. In general, the strong spectral features of most degenerate dwarfs produce adverse effects in the color indices obtained with the standard systems (see Weidemann 1963 for effects in the UBV bands) rendering inconclusive results.

In order to examine the distribution of degenerate dwarfs on the H-R diagram an accurate temperature calibration is required. At a time when the uncertainty in the luminosity of the degenerate stars is being reduced drastically by several parallax programs now in progress, an improved temperature calibration becomes compelling.

It is expected that the u, s, β, and y system can provide a satisfactory temperature calibration in order to study the observable effects of the energy balance in white dwarfs, especially those effects resulting from the crystallization hypothesis.

CHAPTER 2

INSTRUMENTATION

At the end of 1971 Dr. Donald J. Taylor finished
the construction and tests of an area and spectrum scanner
of his own design. Observational results obtained with
that instrument have been published by Spinrad, Smith and
Taylor (1972). By removing the monochromator the same
instrument can be used as a single channel photometer
capable of star-sky chopping and rapid alternation of
the filters. The optical characteristics and the dimen-
sions of the photometer were fitted to the F/9 focal
ratio of the Steward Observatory 228-cm reflector.
During 1973 the photometer was equipped with a computer
interface. The observational data for this investigation
were obtained with the instrument operated via a mini-
computer. A description of its main features and con-
trols, plus the calibration of the spectral bands, is
presented in this chapter.

Components of the Photometer

The optical system of this photometer is conven-
tional. A diaphragm is placed in the focal plane of the

telescope followed by a small-angle removable microscope used to inspect the centering of the observed object in the diaphragm. With the microscope out of the light-beam the next elements in the optical path are a filter and a field (Fabry) lens. This last element images the telescope primary onto the cathode of an end-on photo-multiplier.

The instrument was designed to reduce two time-dependent errors commonly present in photometric observations: (1) rapid change of the sky background, and (2) instrumental drift due to temperature effects in the detector. The first type of error is reduced by rapid change of the filters and frequent samples of the sky background. The second one can be reduced by placing the detector in a stable refrigeration system.

Filter Wheel

Rapid and repeated cycling of the filters was achieved by mounting them on a wheel geared to a stepping motor that drives the rotation. The filter wheel has room for six filters of 2.6 cm square and up to 0.8 cm thick. Change from one filter to the next can be done in 20 steps of the motor in a minimum time of 0.240 s. The origin of the sequence of filters is marked by a fiducial point on the wheel. During the time that the first filter of the sequence is in the light-beam the

fiducial point closes a circuit that carries an electric signal. That signal is used to start counting the steps of the driving motor. After the signal from the fiducial point has been read once the stepping motor can drive the wheel forward or backward, from the position of any filter, for an indefinite time.

The filter wheel was located 4 cm below the focal plane. At this distance the F/9 beam illuminates an area of about 4 mm in diameter on the filters.

Chopper

Frequent observations of the sky background were made using the area scanner as a chopper, i.e., only discrete linear scans in three positions were allowed. The driving mechanism of the scanner is provided by a loud speaker coil and a permanent magnet. The coil is at the end of a steel shaft, the diaphragm is at the other end. When the coil is energized the shaft slides through two oilite bearings. Position feedback is obtained with a linear variable differential transformer (LVDT). The transformer core is attached to the reciprocating steel shaft. Essentially, the LVDT provides a DC voltage proportional to the displacement from the center position. This voltage is subtracted from a fixed voltage produced by an independent power supply and the difference is fed to a DC power amplifier that energizes the coil.

Accordingly, for a given setting of the independent power supply there is a rest position of the coil. If the coil is forced to a different position the LVDT generates a DC voltage that is used to generate the required power for a return to the rest position. Different rest positions can be repeated to within 0.05 mm; at the 228 cm reflector, in the F/9 mode, such uncertainty corresponds to 0.5".

Three rest positions were defined for the chopper: the center one for observationof the star, and the other two for observations of the sky on both sides of the star. A diaphragm 10" in diameter was used in all the observations, while the separation between the star and sky position was set at 15".

In order to maintain the exit pupil of the optical system immobilized on the detector, a 2.5 cm diameter (F/2.5) Fabry lens was placed 6.4 cm above the cathode. The distance between the focal plane and the Fabry lens is 8.2 cm approximately. When the 10" diaphragm is in the optical axis (star position) a spot 9 mm in diameter is illuminated on the center of the Fabry lens. A displacement of few millimeters on the focal plane produces a similar displacement on the Fabry lens. Sky observations during daytime were performed in order to determine the limit for off axis observations. The results indicate

that the chopper can be displaced 4 mm from the center (40" off the optical axis) without reduction in the signal.

Cryostat

Besides the well-known thermal dark current, there are other thermal effects in photomultipliers that can reduce the accuracy of astronomical photo-electric photometry. In general these effects produce a multiplicative noise, in contrast to the thermal dark current that is an additive noise (Young 1974). One example of multiplicative noise is variations in the spectral responsivity of the cathode and the dynodes. Temperature coefficients of +1% per degree centigrade in the red end are characteristic of many cathode materials. The variations become important on cooling far below the temperature of the surrounding environment, when thermal stability is difficult. Another example of multiplicative noise is variations in the collection efficiency of the dynode string. This happens when the cathode and the dynodes lose electric conductivity at low temperatures and the electric field configuration between the different components is altered. The net effect is a shift in the statistic average of collected electrons.

On these grounds, current ideas in the use of photomultipliers favor more stable and less extreme cooling temperatures.

The observations required in this investigation were obtained with a photomultiplier refrigerated by a thermoelectric (Peltier effect) cryostat. This particular cryostat was tested in the laboratory to determine the lowest temperature of the cooling walls and the amplitude of the temperature fluctuations in the steady state of the thermoelectric system. With the photometer at room temperature (the approximate temperature of summer nights on Kitt Peak) the cooling walls reached -19 C, with hourly fluctuations less than 0.5 C in amplitude. With the instrument in 0 C ambient, the lowest temperature was -22 C. Slow fluctuations of almost 1 C were recorded in this case. The time necessary to reach minimum temperature ranged between three and ten hours. These changes are certainly caused by different rates of heat dissipation of the Peltier elements in different ambient temperatures.

The photomultiplier is hermetically sealed inside the cryostat. A heated window is located about 3.8 cm in front of the cathode. The supports of the window are connected to the body of the cryostat, where the temperature takes an intermediate value between those

of the environment and the cooling walls. The heater dissipates 5 W (at 110 V) and in steady state most of the heat is lost by conduction, leaving the window at about 15 C. The Fabry lens is located 2.6 cm above the window. Due to its proximity to the heated window the Fabry lens was always warmer than 0 C. The thermo-electric system of the cryostat and the window heater were energized at least 20 hours before an observing run started. To preserve temperature stability they were kept working, day and night, until the observing run ended.

The observational results, obtained throughout the four seasons of the year, indicate that the use of the thermoelectric cryostat was sufficient to avoid drifts of the zero point during one night. Changes of 0.01 to 0.03 mag were recorded between different runs.

Computerized Controls

Coordination between the position of the filter wheel, the star-sky chopper, and the integration times was maintained with a Nova 800 minicomputer with 20,000 memory words. Registration of the signal, labeling and storage of the data was also done with the computer. Permanent peripherals used in these tasks were a disk unit, a magnetic tape driver, and a teletype.

<u>Interface</u>

Digital signals between the computer and the photometer were transferred by an electronic interface. One unit of the interface was assigned to link the stepping motor and the fiducial point of the filter wheel with the computer. A second unit was used to drive the chopper. The digital signals from the computer were processed in this unit and transformed into analog signals to feed the voice coil. Another unit was attached to the binary counter used to register the signal from the photomultiplier. The capacity of this unit was 64,000 counts with a maximum counting speed equivalent to 10 MHz.

The main unit of the interface was connected to two control panels. One panel was placed on the observing platform, and the other one in the computer room. Both panels were composed of ten push buttons and a numerical display. Each button was assigned a specific command to control the observations. For instance, one button was used to start and stop an observation; a second one was used to obtain a printout on the teletype of the data from the last observation; a third button produced a pause during an observation in order to check the position of the star in the diaphragm. Several buttons were used to monitor different data (such as

star counts, sky counts, and total integration time) on
the numerical displays.

Software

Programming of the controls and the data handling
was done in FORTH language (Moore 1974). A basic dic-
tionary of 27 definitions was produced to operate the
photometer. Most of these definitions were instructions
to be executed by the components of the photometer. They
were coded to the Nova 800 to be interpreted by the FORTH
assembler. The basic dictionary could be used to pro-
gram a wide range of observing routines and data handling
modes.

In order to provide a permanent access to these
definitions, once the basic dictionary was loaded, two
major tasks were run simultaneously in the computer.
One task was to sense the push buttons every 0.1 s,
independently of the teletype. The second task was to
perform the observing routine. At the moment that the
start push button was "on," the second task was initiated.
Then, data acquisition was performed in repeated cycles.
When the start push button was sensed "off" by the first
task, the second task stopped at the end of a cycle.

This programming mode is suitable for the opera-
tion of the photometer by only one person located next
to the instrument or in the computer room.

Photomultiplier Operation

A photomultiplier with a S-20 spectral respon-
sivity and manufacturer designation D 224 was used in
the photometer. This tube is an adaptation of the EMl
9558 photomultiplier, with a focusing electrode that
funnels photoelectrons from a circle (up to 1 cm in
diameter) in the center of the cathode into the first
dynode. Thermionic emission from outside the active
center of the cathode is screened by a mask in front of
the first dynode. Under a given set of operational con-
ditions, the optimum voltage for the focusing electrode
corresponds to the collection of photoelectrons from the
illuminated area of the cathode only. The anode signal-
to-noise ratio is highly dependent on this effect and
can be used to determine the optimum voltage. Regulation
of the focusing electrode is provided by a reostat
placed in the socket of the tube.

The principal detection methods used with photo-
multipliers have been analyzed by Young (1969). The
methods used in astronomical observations are (1) dc
current or voltage measurements, (2) charge integration,
and (3) pulse counting. These methods are possible,
and in fact, they are not far from the optimum detection,
because the anode output is a pulsed current. The essen-
tial difference between these detection schemes is the

weighting function applied to the pulse registration. In dc techniques each pulse is weighted by its height (measured as charge or voltage); in pulse counting all pulses within a range of heights are given weight unity, and the remaining pulses are ignored. When digital techniques are used in the general operation of a photometer it is advantageous to use pulse counting.

The operation of our D 224 photomultiplier was in the pulse counting mode. A Spacom-135 voltage sensitive pulse amplifier and discriminator was connected to the anode of the photomultiplier. Maximum and minimum sensitivities of the amplifier are 0.11 and 3.16 mV respectively. At maximum gain the discriminator is recommended for frequencies below 12 MHz, according to the manufacturer. This implies that the resolution time of the discriminator is about 83 ns. The amplifier discriminator system produces one standard output pulse of 2.9 V amplitude and 53 ns width. The output pulse was carried to the counter by a coaxial cable with matched impedance at both ends. The threshold of the discriminator can be monitored with special output voltage that ranges between 0 and +4 V. The actual threshold is approximately proportional to the inverse square of the output voltage. No discriminator is provided for high pulses.

Settings

     The starting point in the operation of the pulse counting system was to fix the gain of the pulse amplifier. In order to avoid the noise originating in places other than the photomultiplier, the pulse amplifier was set at its maximum gain. After this, the optimum threshold setting was investigated.

     Denoting the rate of anode pulses exceeding the amplitude of the threshold t by n(t), then

$$n_i(t) = \int_t^\infty i(x)\ dx \qquad \text{with } i = s, d\ . \qquad (5)$$

Here $s(x)$ and $d(x)$ are the signal and dark pulse-high distributions, respectively. Light falling on the cathode of the photomultiplier produces the signal distribution $s(t)$. The sum $[n_s(t) + n_d(t)]$ and $n_d(t)$ can be easily measured in a time independent regime. The variation of the rate with respect to the threshold settings gives the pulse-height distribution.

     If the total dynode acceleration potential (high voltage) is increased, the $n_s(t)$ and $n_d(t)$ curves take higher levels. Following Robben (1971), curves of $n_s(t)$ and $n_d(t)$ were obtained for different values of the high voltage. It was observed that the $n_s(t)$ curves become

almost independent of the threshold t at 1500 V. For
higher acceleration potentials $n_s(t)$ increases very slowly
in comparison with the increase of $n_d(t)$; therefore,
1500 V was chosen as the operating high voltage.

The optimum threshold level was determined with
the method derived by Young (1969). In the framework of
this method, the threshold that allows maximum signal-
to-noise ratio is given by the relation

$$2 \frac{s(t)}{d(t)} = \frac{n_s(t)}{n_d(t)} . \tag{6}$$

The value of t that satisfies this relation can be easily
found by plotting both ratios with respect to the thresh-
old settings. The average of several determinations,
with the D 224 tube at 1500 V, indicates that the optimum
threshold is 3.0 $\pm$ 0.1 V in terms of the monitoring
voltage. If the actual threshold is proportional to the
inverse square of the monitoring voltage, the uncertainty
of 0.1 V is equivalent to less than 2% error in the
threshold.

On October 7, 1974, after the observing program
was almost completed, the tube and the pulse counting
system were tested at the Kitt Peak National Observatory
Photomultiplier Laboratory. The tests were made inde-
pendently by Mr. David Stultz using an automatic pulse

analyzer. He found that the optimum high voltage was
1500 V and that the threshold setting should be 2.96 V.
These results corroborate the early determinations and
indicate that the detection system was very stable.

Tests

Aside from the several operational tests mentioned
above the performance of the photomultiplier was investi-
gated for linearity and polarization effects with obser-
vations at the telescope.

Deviations from linear response in a pulse count-
ing system are due to finite resolving time of the circuit.
At low signal levels the rate of registered pulses is
given by

$$n_{reg} = \frac{n}{1 + n\tau} \tag{7}$$

where τ is the resolving (dead) time and n is the rate
of pulses available for counting (Kelley 1964).

The maximum frequencies allowed in our system
have been mentioned above. They correspond to dead times
of 80 ns in the amplifier-discriminator and 100 ns in
the counter. It seems safe to accept 100 ns as the re-
solving time of the system in order to determine the
maximum rate allowed by the system before the number of
lost pulses become comparable to the statistical error

of the signal. According to Equation 7 after an integration time t the number of lost pulses is $(n - n_{reg})t$ = nt τn_{reg}. If we request that the statistical error of the incoming pulses, $\sqrt{nt}$, is about ten times larger than the number of lost pulses, then

$$\sqrt{nt} \geq 10 \text{ nt } \tau n_{reg} \text{ .} \tag{8}$$

Requesting a relative error $\sqrt{nt}$ / nt = 10^{-2}, we find that the maximum rate of registered pulses should be 10^4 counts s^{-1}. The combined optical efficiency of the 228 cm reflector and the photometer, with the Stromgren y filter, is 2.5% approximately. Therefore 10^4 counts s^{-1} are produced by illumination corresponding to V = 11 mag.

The brightest white dwarf in the observing program was 40 Eri B (EG 33) with V = 9.52 mag. The signal rate of this star was 5 x 10^4 counts s^{-1}. For this rate $\sqrt{n} \simeq (n - n_{reg}) \simeq 240$ counts s^{-1}. However, the statistical error is negligible in comparison with the signal, and deviations of linearity, at this level, are unnoticeable. Analysis of the relation between log n_{reg} (obtained with the y filter) and the V magnitude of stars in the photometric sequences of 3C 48 (Penston, Penston and Sandage 1971) and the Selected Area No. 60

(Priser 1974) proved that, between 9.5 and 16.8 mag, response is linear to an accuracy of 0.01 mag. Fainter stars were not observed; however, there is no reason to question an extrapolation of the linear relation for low signals.

Deviations in the response can also be produced by polarized illumination of the photomultiplier. Light transmitted into the first dynode, or simply anisotropy of the cathode can produce significant differences in the response if the polarization has the right orientation (Young 1974). Although it appears that linear polarization is not a common property of white dwarfs, especially in the DA type, interstellar or intrinsic polarization can be significant in standard stars. For this reason several tests were performed to determine the effect of linear polarization in the D 224 photomultiplier. Observations of several BL Lacertae objects (with intrinsic linear polarizationof about 10%, generally) were obtained changing the orientation of the photometer by 45 degrees. The results indicate that no significant effect was present. Nevertheless, these results were declared inconclusive after linear polarization observations of some BL Lacertae objects by Serkowski (1974) revealed that their polarized flux can change by significant factors in time scales of 30

minutes. A second test was performed with a beam almost completely polarized. A polarizer sheet, type HN-32, was placed in the telescope beam just above the focal plane. For this polarizer the transmitted beam is 97% polarized at 4000 $\overset{o}{A}$, and more polarized at other wavelengths. Several stars were observed eight times each, with the orientation of the photometer changed in 45 degree steps. The results contain no variations above statistical error of the signal, in the four spectral bands used. After these measurements it was concluded that the photometer is not sensitive to linear polarization.

Radiometric Calibration

The spectral bands used in this investigation are described by their relative spectral responsivity as presented in Appendix A. They were determined by measuring the reflectance of the mirror in the telescope, the filters transmittance, and the detector spectral responsivity normalized to its peak value. These three factors were measured independently and in different dates as described below.

Mirrors

According to the empirical results derived by Hass and Waylonis (1961), the main factors affecting the

reflectance of evaporated aluminum are: the rate of deposition, pressure during the evaporation, and thickness of the deposited film. Pressures above 2×10^{-5} mmHg and evaporation times longer than one minute produce a significant reduction of the reflectance in the ultraviolet. Also, films thinner than 600 Å are highly transparent, while thicker than 1000 Å show excessive surface roughness. In both cases the result is low reflectance over the ultraviolet and optical spectrum.

The two mirrors of the Steward Observatory 228 cm telescope were aluminized on July 29, 1974. Several pieces of glass were simultaneously aluminized in order to have sample mirrors to measure the reflectance. The aluminization conditions, for the telescope and sample mirrors, were set at their optimum values: evaporation time 30 s; pressure 5×10^{-6} mmHg; thickness 700 Å.

Two weeks after the deposit the reflectance of the sample mirror was measured in a Cary spectrometer at Kitt Peak National Observatory. The results confirmed high ultraviolet reflectance and a maximum of about 87% reflectance at 5000 Å. The samples were kept in the dome with the telescope and remeasured after six months. Although the maximum reflectance was only 85% this time (apparently due to deposits of dust) the wavelength dependence was unchanged. The square of the reflectance,

i.e., the effect of reflections by two mirrors, was derived and is presented in Appendix A.

Filters

The u and y filters used were u and y ones of the Stromgren four-color system. The Steward Observatory set is one of the 50 matched sets distributed by Kitt Peak National Observatory in 1970. Detailed transmittance of these two filters have been published by Crawford and Barnes (1970). The s (λ~4600 $\overset{o}{\text{A}}$) and β filters were purchased specially for this investigation. Both are interference filters with no transmission leaks in the 3000 to 9000 $\overset{o}{\text{A}}$ region, where the detector described below is more sensitive.

The transmittance of these four filters were measured several times during 1974, with the Cary spectrometer at Kitt Peak National Observatory. In two occasions the filters were measured after a day of cooling, to about 0 C, in a refrigerator. Variations up to 4% in the transmission with respect to the transmittance obtained at room temperature were measured. These results indicate a mild effect of temperature in the four filters, at least in the 0 to 25 C range. From the several measurements it was concluded that the transmittance is known within 2% for any of the four filters. Individual parameters of the filters are presented in

Table 1. Half bandwidth corresponds to the width at 50% transmittance and the equivalent width corresponds to the width of a band with 100% transmittance, centered at the peak wavelength, with integrated transmission equal to the integrated transmission of the filter.

Table 1. Filters' characteristics.

Parameter		Filter			
		u	s	β	y
Peak wavelength	Å	3450	4607	4850	5515
Half bandwidth	Å	390	170	350	220
Equivalent width	Å	169	110	240	214
Peak transmittance	%	42	64	65	87

Detector

The relative spectral responsivity of the detector was measured by Mr. David Stultz (1974) at the Kitt Peak National Observatory Photomultiplier Laboratory. The D 224 tube was maintained in the thermoelectric cryostat; therefore, the resultant responsivity includes

the transmittance factors of the window and the Fabry
lens. The normal operational conditions were used:
cooling temperature at 20 C; high voltage at 1500 V;
threshold monitor at 3 V. Measurements were made at five
wavelengths between 4000 and 8000 $\overset{o}{A}$. The source of radia-
tion was an incandescent lamp at 2000 K, with narrow
band filters selecting the calibration wavelengths.
The relative radiation transmitted by each narrow band
was compared with the signal of the detector to obtain
monochromatic responsivity.

For the ultraviolet region the spectral re-
sponsivity was obtained from data provided by the manu-
facturer. Although the manufacturer measurements were
made at room temperature, there are no reasons to suspect
significant changes for low temperatures. For trialkali
cathodes (S-20 responsivity) the ratio of -18 C to room-
temperature sensitivity has been found to be almost
independent of wavelength in the ultraviolet region
(Young 1963).

The data from the two spectral regions were
matched at 4000 $\overset{o}{A}$ in order to produce interpolated values.
In Appendix A the spectral responsivity, relative to its
maximum value, is listed from 3100 to 7700 $\overset{o}{A}$.

CHAPTER 3

OBSERVATIONS

The observations were obtained on 16 different
dates between February 1974 and January 1975. Only nights
that started with good photometric conditions were used.
On three dates the observations were suspended due to
suspected or evident deterioration of the photometric
quality of the atmosphere. The final results are presented
in this chapter preceded by a description of the observing
program and a discussion of the reduction techniques.

Observing Program

The original observing program was assembled from
well-known DA white dwarfs selected according to two
levels of priority: first, stars with measured trigono-
metric parallax larger than 0."040, and second, stars
brighter than 15th magnitude. With the program in pro-
gress other degenerate stars were also observed; they
include DO, DC, and circularly polarized stars. The
results obtained with these stars demonstrate the advan-
tages of a photometric system tailored to DA white dwarfs.

Standards

In order to monitor the stability of the equip-
ment, determine the atmospheric extinction, and transform
the y magnitude into the standard V system, a series
of bright (V ≃ 10 mag) stars were chosen as standards.
They were selected from the list given by Peterson (1970),
the Selected Area stars observed by Priser (1974), and
the secondary standards published by Philip and Philip
(1973). Although none of these stars are primary stand-
ards their visual magnitude is expressed in the standard
V system and there is no indication that any of them is
variable. Special care was taken to include stars in
a wide range of color indices. The bluest star selected
was BD +28° 4211 (spectral type sd O7p and (B-V) =
-0.37 mag). These pseudo standard stars were observed
at regular intervals between the observations of white
dwarfs; therefore, all the parameters derived with their
observations should be applicable to the program stars.

Routine

The same observing routine was employed through-
out the program. The four filters were alternated in
cycles according to the sequence: y, β, s, u, u, s, β, y.
An observation was ended only after the y filter was
sampled an even number of times. During the time that
a given filter was in the beam the sky was sampled 15"

north and 15" south of the star. The sequence followed
in the observation of the star and the sky is illustrated
in Figure 4.

The total observing time of the star equals the
observing time of the sky (= 4 x DT). This sampling
mode over-observes the sky when bright stars are measured.
For optimum efficiency the star observing time and the
sky observing time should be proportional to the statisti-
cal errors of their respective signals (Young 1974).
Accordingly, equal observing times correspond to stars
that are as bright as the portion of the sky included in
the diaphragm. This situation is approached if observa-
tions of faint stars are obtained during occasions of
significant scattered moonlight in the atmosphere. In
our program such occasions were encountered very often,
and mainly for this reason it was decided to maintain
equal observing time for the star and the sky.

Common values of DT were: 0.25, 0.5, 1, 2, and
4 s. The longer intervals were used with fainter stars
in order to reduce the amount of time spent on filter
changes and motion of the chopper.

During the course of one observation, the
statistical error, i.e., square root of the star counts
integrated in the least efficient spectral band, was
monitored. Normally, after it reached 1% of the
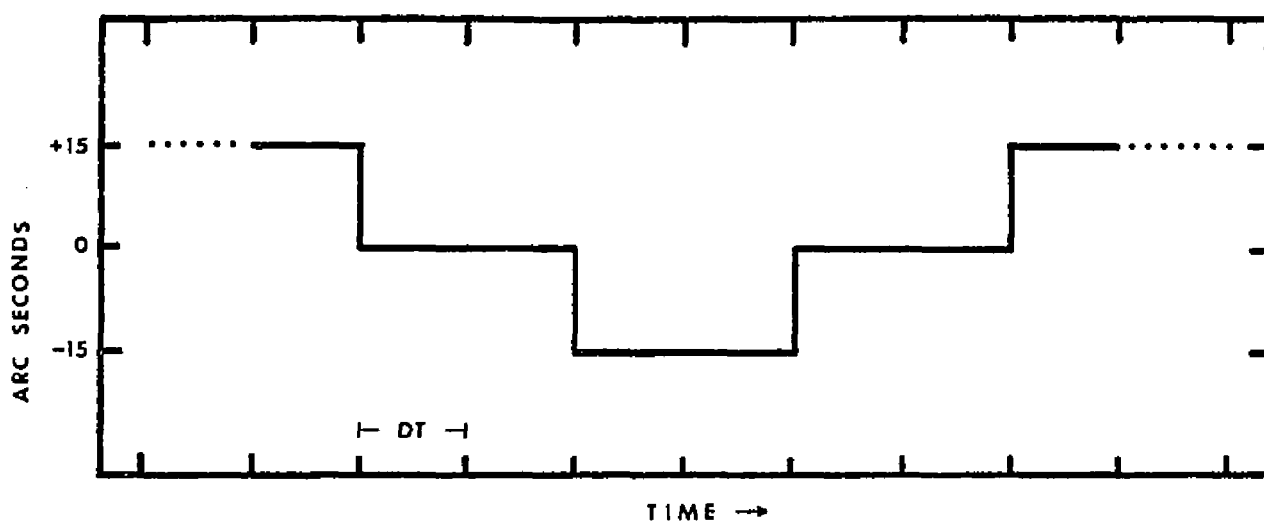
Figure 4.   Sequence of star and sky observations. -- The
             line shows, schematically, the position of the
             diaphragm during the observation with a given
             filter. The star is observed in position 0
             arc seconds. Sampling of the sky was made 15
             arc seconds north and south of the star. The
             dotted lines indicate observations with a
             different filter.

integrated signal the observation was stopped. The data collected were stored by the computer on the disk and after the observation ended the data from the four bands were displayed for inspection. For each observation the computer stored also the Universal Time of start and end, and the Local Siderial Time corresponding to the mean.

At the end of an observing run, the complete body of observations was copied into a magnetic tape for more permanent storage. As a backup, a printout of the observations was also obtained. This printout was later used to start the reductions.

Data Reduction

The reductions were performed with a Hewlett Packard 9810A calculator. The first step was to transform the data of each observation into magnitudes and colors. For this purpose the following relations were used:

$$m = 2.5 \log(n_y) + 22.0 \qquad (9)$$

and

$$(i-j) = 2.5 \log(n_i/n_j) \qquad (10)$$

with $i \neq j$; $i = u, s, \beta$ and $j = s, \beta, y$. Here n_y, n_i, and n_j are the registered rate of counts from the star

free of sky background. The magnitude observed in the y
band is denoted by m and (i-j) represents the color index
between two different bands. In a second step, the air
mass of each observation was computed with the (corrected)
formulae given by Schulte and Crawford (1961).

The rest of the reductions were made with equa-
tions that redress the effect of atmospheric extinction
and place the magnitude and color in homogeneous scales.
To determine the coefficients of those equations only
the observations of the stars considered as standard
were used.

Extinction

The extinction coefficients were determined with
the method derived by Stock (1969) for wide-band photome-
try. This method assumes that the extinction is linearly
dependent on the colors, and requires observations of
stars separated by about four hours of Right Ascension
in order to obtain data at optimum air masses. For this
purpose the photometric sequences in Selected Areas
(Priser 1974) were used. Determination of the extinction
coefficients was pursued every observing night of the
program. Independent determinations were obtained in
13 of the 16 dates. Values of the coefficients are pre-
sented in Table 2. Mild color-dependence of the extinc-
tion (b = -0.015) was found in the magnitude m and the

Table 2. Extinction coefficients.

	y		(u-s)		(s-y)		(s-β)	(β-y)
	a	b	a	b	a	b	a	a
	mag	mag	mag	mag	mag	mag	mag	mag
1974								
Feb 2	0.213	−0.014	0.44	−0.01	0.061	−0.030	0.058	0.044
Feb 3	0.199	−0.013	0.44	−0.02	0.061	−0.030	0.046	0.047
Mar 11	0.236	−0.012	0.49	−0.014	0.104	−0.034	0.070	0.059
Apr 30	0.222	−0.011	0.482	−0.016	0.094	−0.029	0.058	0.047
May 1	0.234	−0.012	0.483	−0.024	0.106	−0.027	0.066	0.048
Jun 8	0.194	−0.020	0.452	−0.032	0.095	−0.033	0.059	0.049
Jun 9	0.194	−0.021	0.465	−0.035	0.103	−0.033	0.069	0.044
Jun 28	0.210	−0.015	0.49	−0.01	0.100	−0.033	0.037	0.050
Jun 29	0.210	−0.015	0.49	−0.01	0.100	−0.033	0.036	0.050
Aug 28	0.208	−0.004	0.50	−0.01	0.103	−0.041	0.051	0.049
Sep 9	0.335	−0.018	0.62	−0.01	0.165	−0.041	0.066	0.087
Nov 4	0.165	−0.020	0.475	−0.028	0.080	−0.020	0.054	0.031
Nov 5	0.168	−0.005	0.45	−0.013	0.070	−0.032	0.056	0.021
Nov 25	0.186	−0.015	0.45	−0.01	0.087	−0.025	0.068	0.064
Dec 3	0.206	−0.015	0.44	−0.01	0.089	−0.022	0.064	0.050
1975								
Jan 22	0.186	−0.015	0.58	−0.04	0.082	−0.025	0.064	0.055

(u-s) color. Significant dependence (b ≃ -0.030) is present in the extinction of (s-y).

The extinction color dependence of (s-β) and (β-y) was found insignificant when derived with observations of standard stars. However, due to the strong absorption lines of the white dwarfs it was uncertain that the color independence could apply to the program stars also. Therefore, the extinction coefficients for (s-β) and (β-y) were determined with observations of white dwarfs. The result in this case was similar to that found with the standard stars; hence it was decided that b = 0.0 for the two color indices involving β.

In the lines of the Stock method, values of the magnitude m and the color indices free of atmospheric extinction were obtained with the following equations.

$$m_o = m - \{a + b\ (s-y)_o\}\ X \tag{11}$$

and

$$(i-j)_o = \{\tfrac{a}{b} + (i-j)\}\ e^{-bX} - \tfrac{a}{b} \tag{12}$$

with $i \neq j$; i = u, s, β, and j = s, β, y. In these two equations the subindex zero labels the values at air mass X = 0.0 (i.e., free of atmospheric extinction).

Transformations

The resultant values of m_o and $(i-j)_o$ were analyzed for night-to-night drift of the zero point in the scale of magnitudes. A clear relative shift was found in the observations obtained after the realuminization (29 July 1974), evidently caused by the new reflectance of the telescope mirrors. For a finer analysis of the night-to-night drift the data were divided into those observations obtained before and after the aluminization date.

Relative shifts in the zero point of m_o as large as 0.03 mag were found in both periods. For each period the night with more observations of standard stars was selected as a reference night and the rest of the nights were corrected by their zero point shift. After that, the following transformations of m_o to the standard V system were found. For observations of the first period (labeled with the superscript I):

$$V = m_o^I - 1.741 - 0.07\,(s-y)_o^I; \qquad (13)$$

and for observations of the second period (superscript II):

$$V = m_o^{II} - 0.682 - 0.06\,(s-y)_o^{II}. \qquad (14)$$

The situation with the color indices is of similar character. However, in this case it was decided to transform the data from the first period to the zero point and scale of the observations obtained in the second period. The transformation equations were the following:

$$(u-s)_o^{II} = -0.052 + 1.102 \ (u-s)_o^{I} \ ,$$

$$(s-y)_o^{II} = -0.074 + 1.044 \ (s-y)_o^{I} \ ,$$

$$(s-\beta)_o^{II} = -0.026 + 0.955 \ (s-\beta)_o^{I} \ ,$$

$$(\beta-y)_o^{II} = -0.084 + 0.945 \ (\beta-y)_o^{I} \ . \tag{15}$$

A final transformation step is required in order to eliminate zero point shifts due to the arbitrary values assumed for the zenith air mass and the neutral extinction. Observations obtained outside the atmosphere should be free of such systematic error and a direct comparison with our colors would be sufficient to derive the amount of the shift. At the present time a possible way to determine the zero point shift is to make use of the energy distributions of several white dwarfs observed by Oke (1974) and Greenstein (1974a). Those

energy distributions have been published at numerous wavelengths and can be integrated in our four spectral bands (see Appendix A) to derive outside of the atmospheric colors. However, the data is based on the absolute calibration of Vega provided by Oke and Schild (1970), which, as documented by Mihalas (1975), is affected by overestimated ultraviolet extinction. The necessary correction has been derived by Hayes and Latham (1975) after an apparently accurate consideration of the different components in the atmospheric extinction.

Accordingly, the data of the seven stars listed in Table 3 were corrected by the amount prescribed by Hayes and Latham (1975) and the resultant energy distributions were integrated in the u, s, β, and y bands to produce outside of the atmosphere colors. As expected, the differences between the synthetic and the observed colors were found to be independent of the stars' colors. The final transformations to outside of the atmosphere are given by the following equations.

$$(u-s) = (u-s)_o^{II} + 0.095 \ ,$$

$$(s-y) = (s-y)_o^{II} - 0.314 \ ,$$

$$(s-\beta) = (s-\beta)_o^{II} - 0.041 \ ,$$

$$(\beta-y) = (\beta-y)_o^{II} - 0.375 \ . \tag{16}$$

52

Table 3. Zero-point-check stars.

EG No.	Sp. T.	(B-V)	Energy Distribution Ref.
50	DA	-0.08^m	Oke (1974)
86	DO	-0.36	Oke (1974)
98	DA wk	-0.10	Oke (1974)
139	DA	-0.07	Oke (1974)
148	DC	+0.17	Oke (1974)
247	DA wk	-0.32	Oke (1974)
290	DCP	+0.62	Greenstein (1974a)

The uncertainties of the zero point for the colors as derived from the seven stars in Table 3, are ±0.021 mag for the (u-s) color and less than ±0.010 mag for the other three colors. A possible cause for the larger uncertainty in the ultraviolet region could be an incorrect spectral responsivity of the detector. At the present time practical difficulties with the calibration of the photomultiplier preclude a reduction of the uncertainty attached to the u band.

Photometric Results

The resultant V magnitudes and the four color
indices of the DA white dwarfs included in our program
are presented in Table 4. The first column gives the
number of the star in the sequence established by
Greenstein (1974b). A cross reference to original names
and other designations has been published by McCook and
Sion (1977). The uncertainties quoted for the V magni-
tude and the colors correspond to the standard deviation
of one observation. The last two columns give the number
of observations and the spectral type, respectively.
Spectral types are reproduced from the series of papers
by Greenstein. Only individual observations obtained in
different nights have been considered to derive the re-
sultant data. When one star was observed more than once
during a night, the observation with the smallest air
mass was selected as representative of that night. The
averages of the values of V were obtained with weight
unity for each observation. In the case of the colors
the averages were computed by weighting the individual
observations with the inverse square of the air mass.
This weighting mode is dictated by the variation of the
statistical error of the signal with air mass (Stock 1969).

Table 5 presents the photometric results of the
non-DA degenerate dwarfs included in our observing program.

Table 4. The u, s, β, and y photometry of DA white dwarfs.

EG No.	V	± σ	(u-s)	± σ	(s-y)	± σ	(s-β)	± σ	(β-y)	± σ	n	Sp.T.
10	14.17		-0.325		-0.708		0.262		-1.049		1	(DA)
11	12.86	0.01	-0.399	0.020	-0.412	0.020	0.506	0.030	-1.017	0.030	5	DAs
15	13.21	0.01	-0.816	0.016	-0.827	0.016	0.293	0.015	-1.214	0.017	3	(DA)
17	13.59		-0.905		-0.852		0.290		-1.261		1	(DA)
26	14.46	0.01	-0.509	0.016	-0.804	0.014	0.251	0.005	-1.145	0.010	3	DA
28	13.74	0.01	-0.445	0.016	-0.720	0.012	0.286	0.004	-1.099	0.016	4	DA
29	15.24	0.02	-0.551	0.020	-0.782	0.018	0.251	0.011	-1.137	0.021	2	DA
30	14.11		-0.405		-0.752		0.257		-1.129		1	DA
33	9.49	0.02	-0.581	0.030	-0.802	0.047	0.276	0.003	-1.170	0.002	5	DA
34	15.65		-0.375		-0.756		0.326		-1.205		1	DAs
36	14.26	0.01	-0.839	0.032	-0.819	0.019	0.298	0.025	-1.220	0.009	2	(DA)
37	13.99	0.01	-1.023	0.032	-0.847	0.013	0.301	0.019	-1.257	0.005	2	(DA)
38	13.78		-0.555		-0.468		0.396		-0.970		1	DAe
39	14.14		-0.895		-0.838		0.328		-1.263		1	DA
42	13.82	0.04	-1.152	0.046	-0.872	0.026	0.319	0.035	-1.300	0.088	2	DAn
46	13.49	0.05	-1.097	0.038	-0.850	0.031	0.311	0.020	-1.281	0.034	3	DA
50	11.85	0.02	-0.926	0.038	-0.861	0.022	0.292	0.003	-1.245	0.019	4	DAn
67	13.29	0.02	-0.379	0.012	-0.778	0.012	0.279	0.009	-1.156	0.014	6	DA
70	13.01		-1.075		-0.892		0.305		-1.285		1	DAn
76	13.06	0.02	-0.559	0.020	-0.788	0.001	0.273	0.009	-1.174	0.003	4	DA
83	13.68	0.03	-0.565	0.007	-0.792	0.012	0.289	0.014	-1.168	0.030	4	DAs
87	13.25	0.03	-0.157	0.040	-0.349	0.021	0.379	0.024	-0.860	0.025	4	(DA)
99	13.33	0.03	-0.479	0.039	-0.773	0.020	0.262	0.021	-1.162	0.025	6	DA
102	12.81	0.03	-0.890	0.040	-0.860	0.060	0.302	0.021	-1.247	0.025	6	DA
115	14.38	0.01	-0.345	0.011	-0.665	0.007	0.312	0.008	-1.073	0.015	5	DA

Table 4. -- <u>Continued</u>.

EG No.	V	± σ	(u-s)	± σ	(s-y)	± σ	(s-β)	± σ	(β-y)	± σ	n	Sp.T.
123	14.36	0.02	-0.343	0.012	-0.753	0.012	0.270	0.008	-1.125	0.005	3	DA
125	13.94	0.04	-0.355		-0.789		0.285		-1.170		1	DA
130	14.11	0.01	-0.397	0.015	-0.816	0.019	0.248	0.019	-1.158	0.017	2	DAn
131	12.28	0.01	-0.921	0.003	-0.611	0.001	0.501	0.028	-1.204	0.002	2	DAwk
135	13.62	0.05	-0.418	0.039	-0.453	0.025	0.439	0.020	-1.071	0.028	3	DAs
139	11.55	0.03	-0.843	0.040	-0.852	0.020	0.298	0.020	-1.242	0.027	5	DA
150	12.84	0.07	-0.711	0.037	-0.828	0.029	0.267	0.033	-1.228	0.022	5	DA
155	14.34	0.01	-0.546	0.026	-0.639	0.017	0.339	0.034	-1.085	0.040	4	DA
159	12.97	0.04	-0.433	0.031	-0.717	0.003	0.275	0.007	-1.077	0.013	3	DA
161	15.32		-0.415		-0.615	::	0.286		-0.989		1	DAn
162	12.94	0.02	-0.425	0.035	-0.748	0.001	0.260	0.019	-1.199	0.022	2	DA
168	14.47	0.01	-0.416	0.017	-0.436	0.007	0.496	0.009	-1.063	0.007	3	DAs
184	12.51	0.04	-0.909	0.004	-0.851	0.026	0.270	0.021	-1.221	0.030	4	DAwk
199	14.28	0.04	-0.314	0.030	-0.342	0.026	0.502	0.035	-0.985	0.038	2	DAss
201	12.97	0.04	-0.482	0.038	-0.794	0.022	0.248	0.025	-1.138	0.030	4	DAn
203	13.79	0.06	-1.360	0.013	-0.908	0.020	0.337	0.010	-1.348	0.037	2	DAwk
232	13.67	0.01	-0.867	0.025	-0.720	0.039	0.305	0.008	-1.144	0.026	2	DA
247	11.75	0.01	-1.456	0.042	-0.932	0.008	0.347	0.006	-1.381	0.007	2	DAwk
261	13.10	0.08	-0.426		-0.780		0.249		-1.097	0.048	1	DA
283	15.51	0.02	+0.025	0.040	-0.166	0.017	0.615	0.014	-0.908	0.011	4	DF
G69 -31	16.15		-0.57		-0.554		0.369		-1.014		1	DA
G76 -48	15.96		-0.34		-0.392		0.460		-0.941		1	DAwk

Table 5. The u, s, β, and y photometry of non-DA white dwarfs.

EG No.	V	± σ	(u-s)	± σ	(s-y)	± σ	(s-β)	± σ	(β-y)	± σ	n	Sp.T.
9	13.74	0.03	-0.754	0.046	-0.531	0.028	0.459	0.035	-1.127	0.038	2	DC
45	14.45		+0.511		-0.730		0.775		-0.831		1	DKe
52	14.59	0.03	+0.897	0.063	-0.756	0.028	0.667	0.031	-0.784	0.025	4	DC
54	12.94	0.03	-0.545		-0.085	0.025	0.445	0.059	-1.048	0.034	1	DF
71	11.21	0.03	-1.517	0.005	-0.913	0.017	0.378	0.021	-1.371	0.026	4	DO
86	14.75	0.07	-1.479	0.026	-0.884	0.040	0.371	0.042	-1.369	0.108	4	DO
95	15.73	0.04	+0.535	0.025	-0.072	0.030	0.611	0.020	-0.883	0.037	3	DC
129	13.21	0.01	-0.937	0.008	-0.598	0.008	0.493	0.005	-1.211	0.009	4	λ4135
148	13.24	0.04	-0.716	0.037	-0.521	0.010	0.511	0.004	-1.109	0.037	5	DC
180	12.34	0.04	-0.444	0.031	-0.376	0.024	0.549	0.039	-1.067	0.029	3	DC
202	16.64	0.07	+1.455		+0.203	0.061	0.734	0.032	-0.604	0.032	3	DC
250	13.80	0.03	-0.418	0.020	-0.412	0.008	0.542	0.009	-1.059	0.010	6	DC
290	14.10		-0.045		-0.167		0.637		-0.916		1	DAP
329	15.08	0.01	-0.425	0.021	-0.445	0.005	0.506	0.031	-1.091	0.030	2	DC-DF
374	15.51	0.06	-0.185	0.020	-0.242	0.070	0.616		-1.003	0.028	3	DXP

Uncertainties

     In Tables 4 and 5 we have quoted the precision of our observations, i.e., how reproducible are the data registered by our instrument. The standard deviation attached to one observation was computed after all the reductions were made; therefore, random errors introduced by the extinction corrections and the transformations are included in the quoted uncertainty.

     The average of the quoted standard deviations for the colors provides an estimate of the uncertainty for those stars with only one observation. These uncertainties are: 0.022 mag in $(s-y)$; 0.030 mag in $(u-s)$; 0.020 mag in $(s-\beta)$; and 0.029 mag in $(\beta-y)$.

     In the case of the V magnitude, it is possible to estimate an external error by comparison with photometric results found in the literature. For this purpose we have selected three different sets of observations obtained under apparently independent conditions. They are: (1) the V magnitudes published by Eggen and Greenstein (1965a, 1965b, 1967) and Greenstein (1969); (2) the V magnitudes obtained at the Naval Observatory, Flagstaff station, and published by Priser (1974), Routly (1972), and Harrington et al. (1975); and (3) the observations obtained by Graham (1972). This last set of observations was obtained with the y filter of the

Stromgren system; however, the corresponding magnitude
is by definition the standard V magnitude. Comparison
of these sets of observations with our data has been
made in terms of the average absolute difference, defined
as $\Delta = \sum |V_a - V_b|/N$, where N is the number of common
stars in the two sets which visual magnitudes have been
labeled V_a and V_b respectively. The results are pre-
sented in Table 6. They indicate that an absolute differ-
ence of about four hundredths of a magnitude is found in
the comparison of any two sets of observations. The
moderate increase of the absolute difference with the
number of common stars appears to be caused by the inclu-
sion of fainter stars. Therefore, for the sample of
white dwarfs included in this investigation the external
error of the V magnitude is 0.04 mag approximately.

Table 6. External errors of the V magnitude.

V_a	V_b	Δ	N
		(mag)	
E and G	This work	0.058	42
Graham	This work	0.045	27
Naval Obs.	This work	0.049	19
E and G	Graham	0.044	28
E and G	Naval Obs.	0.040	17
Graham	Naval Obs.	0.030	10

CHAPTER 4

GRAVITY AND TEMPERATURE DETERMINATION

Several attempts to analyze photometric observations of DA white dwarfs with computed model atmospheres are registered in the literature. Terashita and Matsushima (1969), and Strittmatter and Wickramasinghe (1971) have investigated the UBV photometry. Stromgren's uby colors have been analyzed by Wickramasinghe and Strittmatter (1972), and recently by Wehrse (1975). The same problem was attacked by Shipman (1972) using low resolution scanner observations. Our attempt is presented in this chapter. Gravities and effective temperatures are derived, for 46 DA white dwarfs, from the comparison of observed and computed reddening-free indices.

Model Atmospheres

After the preliminary calculations carried out by Schatzmann (1958), model atmospheres for DA white dwarfs have been computed by several authors in a progressive sequence of refinements. Early computations (Weidemann 1963) assumed a gray temperature distribution and chemical

60

composition of pure hydrogen or hydrogen and helium.
The ratio, by number, between these two elements was
approximated to the value of the (normal) composition
observed in the solar system (Cameron 1973). Non-gray
model atmospheres, with normal hydrogen and helium com-
position, were computed by Terashita and Matsushima
(1966) in which they included the effects of pressure
ionization to determine the emergent flux and the Balmer
line profiles. Improved models, considering hydrogen
blanketing and a small amount of metals in the composi-
tion, were also computed by Terashita and Matsushima
(1969).

The following generation of models for DA white
dwarfs included: more sources of continuous opacity,
accurate corrections to the temperature stratification
in order to maintain a constant flux of energy, and the
effect of pressure ionization on the density of ionized
atoms. As pointed out by Shipman (1972), failure to
account for this last effect produces a reduction of the
electron density which in turn generates weaker absorp-
tion lines. At this level of elaboration we now find
three independent calculations of model atmospheres for
DA white dwarfs. First, Shipman (1972) published eight
models where the ratio, by number, of hydrogen to helium
was made equal to 99/1; second, a series of models for

high temperatures (25000 K $\geq T_{eff} \geq$ 10000 K), with prac-
tically normal composition published by Wickramasinghe
(1972); and third, a series of models at low temperatures
(12000 K $\geq T_{eff} \geq$ 7000 K), published by Wehrse (1976)
where the abundance of elements heavier than oxygen was
reduced by 1/100 with respect to the normal composition.
These last two sets of models share, however, a signifi-
cant degree of homogeneity because in the high tempera-
ture set the heavy metals contribution to opacity was not
included. Consequently, a reduction in the metal
abundance will have insignificant influence on the emer-
gent flux of DA models with $T_{eff} \geq$ 12000 K (Wickramasinghe
(1972).

Convection

Schatzmann (1958) suggested that a convective
zone can exist in some white dwarfs, beginning in the
atmosphere near the surface and extending towards the
interior. Theoretical corroboration for convective
transport of energy in white dwarfs was provided with the
precursory envelope models computed by Van Horn (1970).
Wickramasinghe and Strittmatter (1970) examined the
convective instability in the atmospheric layers of DA
models with log(g) = 8. According to their results, DA
atmospheres are stable between 25000 and 18000 K. At
lower temperature, the incomplete ionization of hydrogen

produces an increase in the opacity and reduction of the
adiabatic gradient, causing some convective transport
of the energy flux. At effective temperatures about
13000 K the atmosphere regains stability as the convec-
tive zone descends below the last observable layers. For
temperatures ranging between 13000 and 8000 K the effect
of internal convection causes an increase of the tempera-
ture in the predominantly radiative atmosphere and
reduces the temperature in the deep convective layers.
As shown by Wichramasinghe and Strittmatter (1970), and
Wehrse (1975) convective models produce bluer color
indices due to the heating of the surface layers.
Nevertheless, the corrections, with respect to pure
radiative models, amount to one or two hundredths of a
magnitude in the UBV and Stromgren colors. According to
these results, convection has a significant influence in
the atmospheric structure of DA white dwarfs; however,
it can be neglected in the analysis of color indices
without important loss of accuracy.

Synthetic Colors

In order to pursue this investigation the grids
of models published by Wickramasinghe (1972) and Wehrse
(1976) were selected to compute theoretical color indices.
These models have been used to investigate the derivation

of atmospheric parameters by Strittmatter and
Wickramasinghe (1971) and Wehrse (1975). A useful aspect
of these models is that the emergent monochromatic fluxes
has been published in a very fine sequence of wavelengths.
This detail is indispensable when accurate theoretical
colors are needed to investigate observational results.
For purpose of our use, the theoretical monochromatic
fluxes F_ν, published by Wickramasinghe (1972), were trans-
formed into flux per unit wavelength.

When well known relative spectral responsivities
$r(\lambda)$ are available, the theoretical colors are computed
with the relation

$$(i-j)_c = -2.5 \log[\int F_\lambda(\lambda) r_i(\lambda) d\lambda]$$

$$x \; [\int F_\lambda(\lambda) r_j(\lambda) d\lambda]^{-1} , \qquad (17)$$

and the integrals are taken from zero to infinity, or at
least over all wavelengths for which the relative re-
sponsivities $r(\lambda)$ do not vanish. These integrations
were performed numerically on the University of Arizona
CDC 6400 computer. In a first step $F_\lambda(\lambda)$ and $r_i(\lambda)$ were
interpolated at intervals of 5 $\overset{o}{A}$ with the double para-
bolic interpolation routine PARCOE described by Kurucz
(1970). For this method, at least four points of a

discrete function are needed. The coefficients of the interpolation parabola are determined by weighting forward and backward parabolas inversely by their second derivatives. Subsequently the terms $F_\lambda(\lambda) \times r_i(\lambda)$ were formed and the integration was obtained with the routine QSF described in the IBM/360 Scientific Subroutine Package (1974). According to the available number of sample points, QSF performs the integration with the Simpson's rule, the Newton's 3/8 rule, or a combination of both. Several tests were made to investigate the accumulated errors of this integration method. The results indicate that the uncertainty in $(i-j)_c$ is of the order 0.001 mag if the discrete function is given at intervals smaller than 10 $\overset{\circ}{A}$.

Values of $(i-j)_c$ are presented in Table 7 for the models computed by Wickramasinghe (1972) and in Table 8 for the Wehrse (1976) models.

Reddening-free Indices

It is well known that the interstellar extinction in the solar neighborhood is not negligible. In a study of the interstellar reddening within 200 pc of the sun, Stromgren (1972) found that for a group of 47 AO type stars the values of E(b-y) range between 0.014 and 0.040 mag in some cases, and larger than 0.040 mag in others. The large values appear to be concentrated in the

Table 7. Synthetic colors obtained with Wickramasinghe's models.

Log(g)	T_{eff} K	$(u-s)_c$	$(s-y)_c$	$\underline{d}$	$(s-\beta)_c$	$(\beta-y)_c$	$\underline{w}$
6	10000	0.025	-0.694	1.069	0.377	-1.071	0.871
	12000	-0.142	-0.768	1.013	0.369	-1.137	0.894
	15000	-0.493	-0.800	0.710	0.394	-1.194	0.946
	20000	-0.845	-0.534	0.409	0.408	-1.242	0.982
	25000	-1.051	-0.856	0.236	0.420	-1.276	1.009
7	10000	-0.242	-0.637	0.716	0.394	-1.031	0.870
	12000	-0.209	-0.750	0.919	0.315	-1.065	0.807
	15000	-0.509	-0.798	0.691	0.349	-1.147	0.879
	20000	-0.854	-0.834	0.400	0.377	-1.212	0.937
	25000	-1.043	-0.563	0.255	0.391	-1.254	0.970
8	10000	-0.495	-0.589	0.391	0.430	-1.019	0.901
	12000	-0.359	-0.696	0.688	0.294	-0.990	0.751
	15000	-0.549	-0.784	0.630	0.288	-1.072	0.783
	20000	-0.869	-0.829	0.378	0.334	-1.163	0.871
	25000	-1.058	-0.860	0.235	0.356	-1.215	0.971
9	10000	-0.673	-0.558	0.166	0.454	-1.012	0.922
	12000	-0.590	-0.624	0.348	0.327	-0.951	0.766
	15000	-0.636	-0.724	0.453	0.234	-0.958	0.676
	20000	-0.904	-0.809	0.312	0.279	-1.088	0.782
	25000	-1.085	-0.848	0.190	0.310	-1.158	0.845

Table 8. Synthetic colors obtained with Wehrse's models.

Log(g)	T_{eff} K	$(u-s)_c$	$(s-y)_c$	$\underline{d}$	$(s-\beta)_c$	$(\beta-y)_c$	$\underline{w}$
8	7000	-0.489	-0.420	0.143	0.572	-0.993	1.031
	8000	-0.506	-0.497	0.241	0.512	-1.009	0.978
	9000	-0.458	-0.562	0.387	0.453	-1.015	0.921
	10000	-0.408	-0.600	0.494	0.409	-1.008	0.875
	12000	-0.390	-0.683	0.639	0.313	-0.997	0.773
8.5	7000	-0.558	-0.212	-0.239	0.627	-0.839	1.015
	8000	-0.557	-0.275	-0.144	0.572	-0.846	0.963
	9000	-0.543	-0.219	-0.214	0.628	-0.847	1.020
	10000	-0.505	-0.359	0.035	0.501	-0.860	0.899
	12000	-0.465	-0.040	0.196	0.431	-0.871	0.834

Scorpio-Ophiuchus and Taurus areas, while the smaller
reddenings are common outside these regions. More
recently, Turon and Mennessier (1975) have studied the
possibility that the Taurus and Ophiucus clouds are linked
by a thin elongated cloud passing about six parsecs from
the sun. The average reddening produced by such clouds
appears to be $E(B-V) = 0.08 \pm 0.04$ mag. Color excess of
such magnitude will produce significant discrepancies in
the observed colors of DA white dwarfs, therefore
reddening-free indices are needed in the derivation of
atmospheric parameters.

In order to determine the effect of the inter-
stellar extinction in the colors obtained with the u,
s, β, y bands the observed energy distributions of four
stars (EG 50, 86, 98, and 247; see Oke 1974) were modi-
fied with the Cygnus extinction law, and the reddened
color computed by numerical integration. Nandy (1968)
has investigated the extinction curves in several galac-
tic regions and concluded that the Cygnus curve appears
to be the average extinction law for the majority of the
stars. In the computations, the Cygnus curve was normal-
ized at 4500 $\overset{\circ}{A}$, and normalization values of one and two
magnitudes were used. The computed color excesses define
straight reddening lines in the (u-s) versus (s-y), and

(s-β) versus (β-y) diagrams. The slopes of those lines give the coefficients used in the following reddening-free indices:

$$\underline{w} = (s-\beta) - 0.462 \ (\beta-y)$$

$$\underline{d} = (u-s) - 1.504 \ (s-y) \ . \tag{18}$$

Reddening-free indices were then obtained with the computed colors of the two sets of models and their values are included in Table 7 and Table 8, respectively. It can be seen that for $\log(g) \geq 7$ the values of $\underline{w}$ reach a minimum around $T_{eff} \simeq 12000$ K, and at the same temperature the values of $\underline{d}$ reach a maximum. In the $\underline{w}$ versus $\underline{d}$ plane these variations display iso-gravity lines that fold over themselves at an iso-temperature line corresponding to $T_{eff} \simeq 12000$ K. For purpose of illustration the overlapping parts of the pattern defined by the reddening-free indices have been separated. The part corresponding to $T_{eff} \geq 12000$ K is presented in Figure 5. Iso-gravity and iso-temperature lines connect the computed values of $\underline{w}$ and $\underline{d}$. The orthogonality of these lines indicates that the $\underline{d}$ index is very sensitive to temperature changes, while it remains almost constant to gravity changes. Similarly, the $\underline{w}$ index is more sensitive to gravity than to temperature changes.

.

Figure 5. The $\underline{w}$ versus $\underline{d}$ diagram for high temperatures.-- Units in the
abscissa and the ordinate are magnitudes. Thick lines connect
computed points of the reddening-free index. Squares are used to
mark the observed points of some DA white dwarfs. Circles are used
for two DO degenerate stars. The EG number has been added for
identification. The short thin line in the lower left side indi-
cates the points computed with power law ($F_\nu \propto \nu^{-n}$) spectra in the
$-0.5 \leq n \leq 3$ range. The long line with small dots corresponds
to the computed points of black-bodies in the $3000 \ K \leq T \leq 500,000 \ K$
range. The uncertainty associated with one observation
($\sigma_w = 0.024$ and $\sigma_d = 0.045$) is presented in the upper left corner.
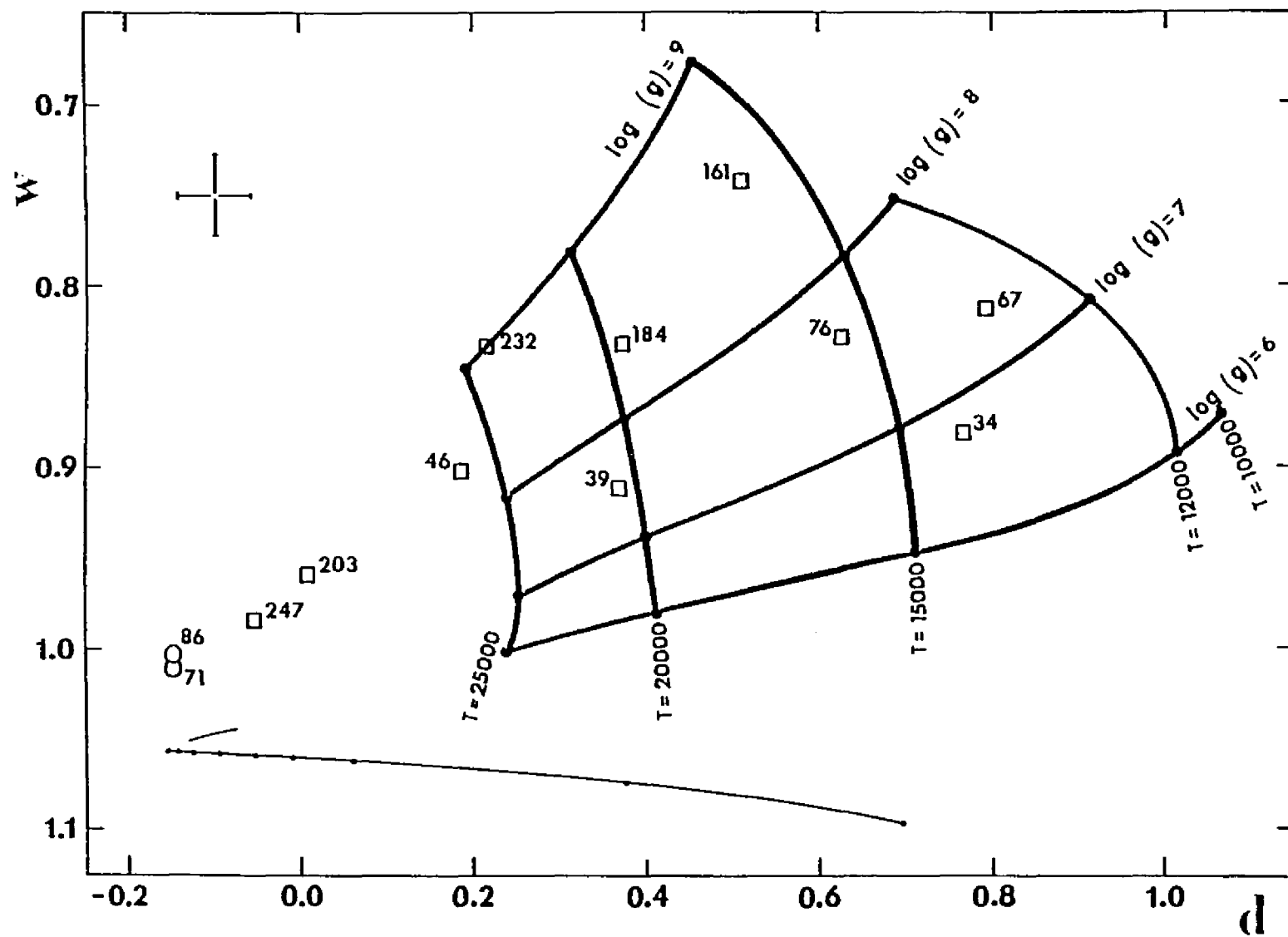
Figure 5. The w versus d diagram for high temperatures.

The pattern corresponding to $T_{eff} \geq 12000$ K is presented in Figure 6 for the models published by Wickramasinghe (1972) and in Figure 7 for the Wehrse's (1976) models. At this point we notice in Figure 6 that the low temperature pattern defined by the computed values of w and d presents a reduced degree of orthogonality with respect to the high temperature pattern (Figure 5). It is also evident that the d index has now lost its sensitivity to the effective temperature, and at the same time has become gravity sensitive. Simultaneously the w index has become less sensitive to gravity and more sensitive to temperature. These changes are caused by the increasing contribution of negative ions of hydrogen to the total opacity, on going from hotter to cooler atmospheres. Because the mean absorption coefficient of H^- is proportional to the concentration of neutral hydrogen and to the electron pressure, in a hydrogen rich atmosphere the onset of H^- opacity is hastened by partial ionization and high gravities. (It is not surprising then that Wildt (1939) was the first to suggest strong H^- absorption in the atmosphere of white dwarfs.) The addition of H^- to the continuum opacity reduces the strength of the Balmer lines making more difficult to detect pressure broadening. The behavior of the w index in Figure 5 reflects this effect. Similarly,

Figure 6.   The w versus d diagram for low temperatures from Wickramasinghe's
          model atmospheres. -- Units, computer points, and the representa-
          tion of the observed points of DA white dwarfs as in Figure 5.
          Circles are used for DC degenerate stars.   Dark squares for
          circular polarized stars.   The triangle represents the observed
          point of EG 129 (spectral type λ4135).   A cross is used for the
          observed point of EG 283 (spectral type DF).   Small digits under
          the black-body line represent the temperature in thousands of
          Kelvin degrees.
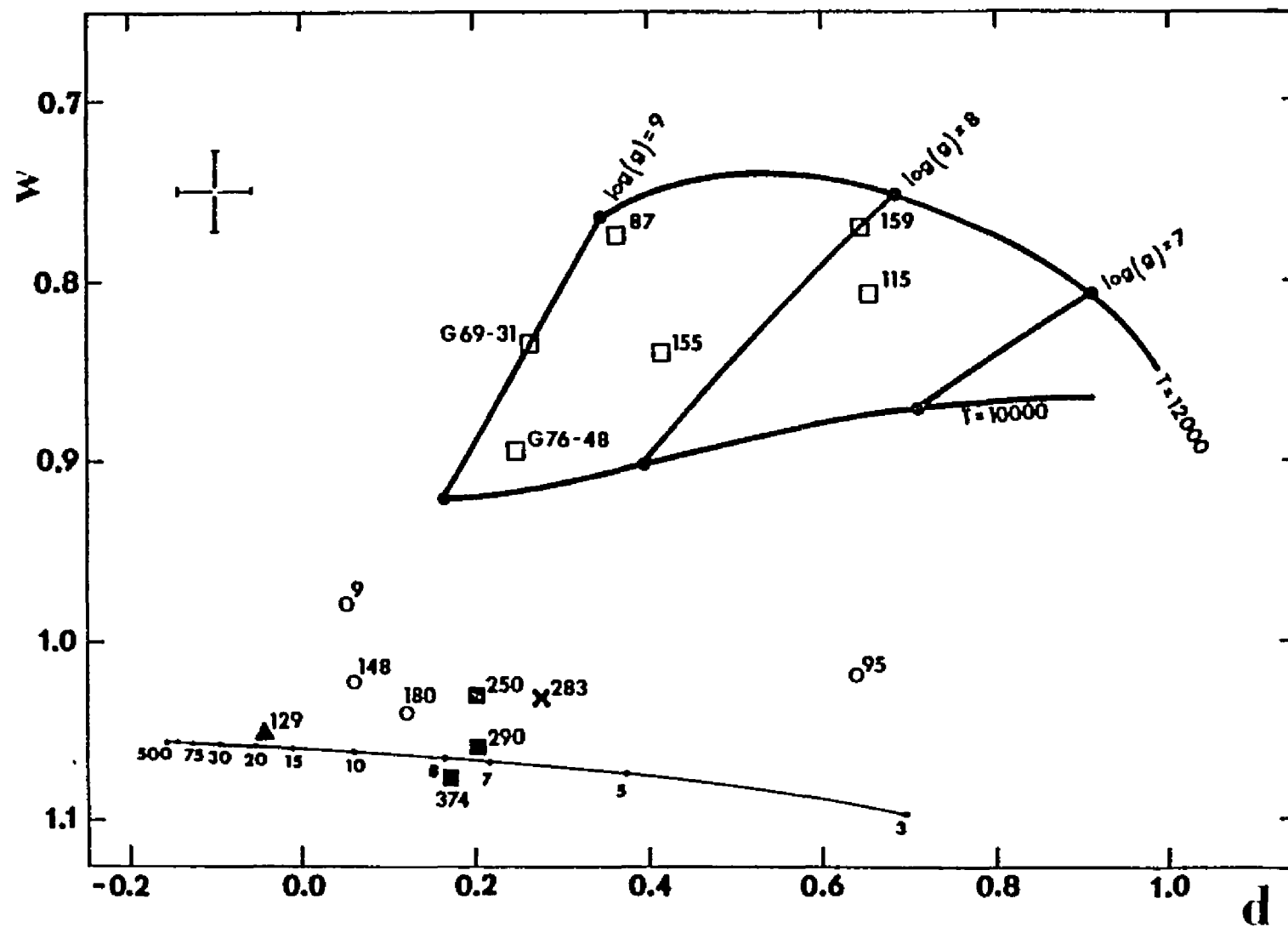
Figure 6. The w̲ versus d̲ diagram for low temperatures from Wickramasinghe's model atmospheres.

Figure 7. The w̲ versus d̲ diagram for low temperatures from Wehrse's model
atmospheres. -- Units, computed points, and the representation of
the observed points of DA white dwarfs as in Figure 5. Dashed
lines are used to connect points of equal temperature. Thin
lines reproduce the low temperature diagram from Wickramasinghe's
model atmospheres, for purpose of reference. Satisfactory agree-
ment between the two sets of models is found for $\log(g) = 8$.
Deviation of Wehrse's published fluxes for $\log(g) = 8.5$ is clearly
visible. The point located below the line for 7000 K corresponds
to the published fluxes for $\log(g) = 8.5$ and $\log(T_{eff}) = 9000$ K.
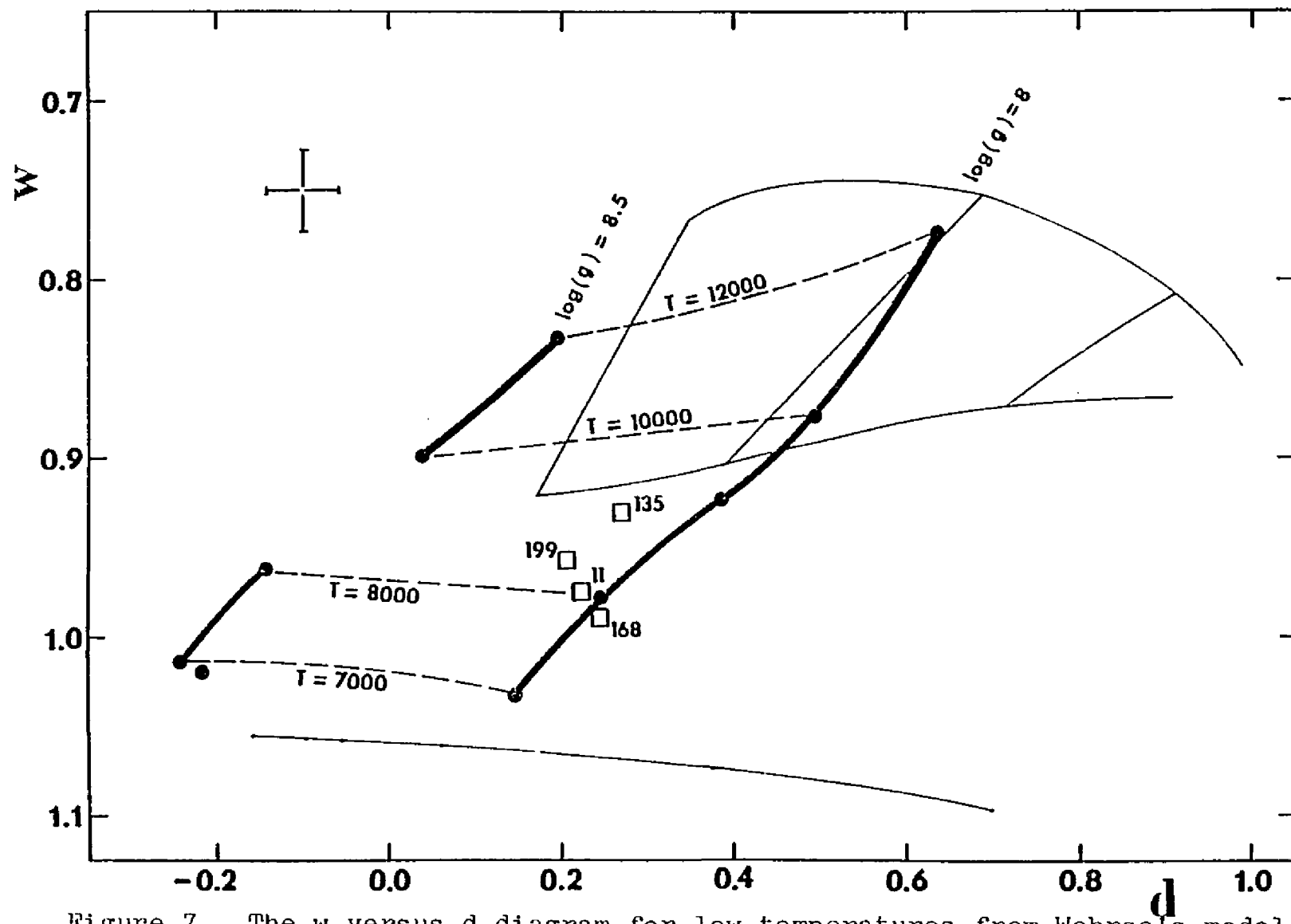
Figure 7. The w versus d diagram for low temperatures from Wehrse's model atmospheres.

H^- in the continuum opacity makes the Balmer jump gravity dependent as indicated by the $\underline{d}$ index in the same figure. The effects of H^- absorption in the standard UBV bands have been analyzed by Weidemann (1963, 1966).

In Figure 7 we note that the values of $\underline{d}$ obtained with Wehrse's (1975) models for $\log(g) = 8.5$ are too blue with respect to the respective values of $\underline{d}$ obtained with the models for $\log(g) = 8$. The effect is produced by the (s-y) color that, as shown in Table 8 is about 0.2 mag redder. The same difference is found in the (b-y) color when the monochromatic fluxes published by Wehrse (1976) are integrated into the u, b, and y bands according to the precepts described by Wehrse (1975). It appears, therefore, that there are some printing errors in the published monochromatic fluxes for the series of models with $\log(g) = 8.5$. In what follows, this series of models will be ignored.

On the other hand, Figure 7 displays remarkable agreement between the models published by Wickramasinghe (1972) and the overlapping (T_{eff} = 12000 and 10000 K) Wehrse's (1976) models for $\log(g) = 8$.

<u>Empirical-theoretical Match</u>

Determination of gravities and temperatures for the observed DA white dwarfs was made on the $\underline{w}$ versus $\underline{d}$ plane. Observed reddening-free colors were derived with

Equation 13 and the color indices presented in Tables 4 and 5. The resultant values fix the coordinates in the $\underline{w}$ versus $\underline{d}$ plane from which values of $\log(g)$ and T_{eff} can be read.

The overlapping regions of the high temperatures (Figure 5) and low temperatures (Figure 6) diagrams create an ambiguity if no previous information on the effective temperature is available. This situation becomes critical for those stars with effective temperature about 12000 K. However, this apparent difficulty is eliminated by the additional information collected by the u, s, β, y bands. In fact, the (u-s) color is strongly dependent on the effective temperature, and can be used to choose the right diagram. No ambiguity is found in Figure 7, where four DA degenerate stars of unmistakably low temperature appear to cluster next to the $\log(g) = 8$ line.

Table 9 presents the observed reddening-free colors and the derived $\log(g)$ and T_{eff} for the DA white dwarfs of our program. The uncertainties quoted for the reddening-free colors are the propagated standard deviations of the observed color indices presented in Table 4. For stars with only one observation of the color indices the corresponding uncertainties are 0.024 mag in $\underline{w}$ and 0.045 mag in $\underline{d}$. Error bars that illustrate these two

Table 9. Reddening-free indices and derived atmospheric parameters for 46 DA white dwarfs.

EG	w	$\pm$m.e.	d	$\pm$m.e.	log(g)	T_{eff} K
10	0.747	0.024	0.709	0.045	8.0±0.2	12000±1000
11	0.976	0.033	0.221	0.036	8.0±0.2	8000±400+
15	0.854	0.017	0.428	0.028	8.0±0.2	19000±600
17	0.872	0.024	0.376	0.045	8.0±0.2	20000±900
26	0.780	0.007	0.700	0.026	7.8±0.1	13500±400
28	0.794	0.008	0.638	0.024	7.9±0.1	15000±500
29	0.776	0.015	0.625	0.034	8.1±0.2	15000±500
30	0.778	0.024	0.726	0.045	7.7±0.2	13000±700
33	0.816	0.003	0.625	0.077	7.7±0.1	15500±1500
34	0.883	0.024	0.762	0.045	7.0±0.4	14000±400
36	0.862	0.025	0.393	0.043	8.1±0.2	19700±700
37	0.817	0.019	0.251	0.038	9.0±0.2	22500±1000
38	0.844	0.024	0.149	0.045	9.2±0.2	26000±1100
39	0.912	0.024	0.365	0.045	7.5±0.3	20600±700
42	0.920	0.029	0.159	0.060	8.3±0.6	27300±2000
46	0.903	0.025	0.181	0.060	8.4±0.4	26400±2000
50	0.867	0.009	0.369	0.050	8.1±0.1	20100±800
67	0.813	0.011	0.791	0.022	7.3±0.1	13100±300
70	0.899	0.024	0.266	0.045	8.2±0.3	24000±1500
76	0.815	0.009	0.626	0.020	7.7±0.1	15500±400
83	0.829	0.020	0.626	0.019	7.6±0.2	16000±500
87	0.776	0.027	0.368	0.051	8.9±0.2	11900±500*
99	0.799	0.024	0.684	0.049	7.7±0.2	14100±800
102	0.878	0.024	0.403	0.050	7.8±0.3	19600±900
115	0.808	0.010	0.655	0.015	7.7±0.2	11300±500*
123	0.790	0.008	0.789	0.022	7.4±0.1	12700±400
125	0.825	0.024	0.832	0.045	7.1±0.2	13000±400
130	0.783	0.020	0.830	0.032	7.3±0.2	12000±400
131	1.057	0.028	0.000	0.003	...±...	15000±500
135	0.933	0.024	0.263	0.054	8.5±0.4	9000±1000+
139	0.872	0.023	0.438	0.050	7.8±0.3	19000±1000
150	0.834	0.034	0.534	0.057	7.9±0.4	17000±800
155	0.840	0.039	0.415	0.033	8.3±0.5	11000±1000*
159	0.772	0.009	0.645	0.031	8.0±0.1	11900±600*
161	0.743	0.024	0.510	0.045	8.6±0.1	16000±600

Table 9. -- <u>Continued</u>.

EG	w	$\pm$m.e.	d	$\pm$m.e.	log(g)	T_{eff} K
162	0.814	0.021	0.700	0.035	7.8±0.2	14000±500
168	0.987	0.010	0.240	0.020	8.0±0.2	8000±500+
184	0.987	0.010	0.240	0.020	8.4±0.3	19700±700
199	0.957	0.039	0.200	0.049	8.5±0.4	8500±400+
201	0.774	0.028	0.712	0.050	7.8±0.2	13000±1000
203	0.960	0.020	0.006	0.033	8:	>30000
232	0.833	0.014	0.216	0.064	9.0±0.2	23900±500
247	0.985	0.007	-0.054	0.044	8:	>30000
261	0.755	0.030	0.747	0.045	7.8±0.3	12000±1000
G69 -31	0.837	0.024	0.263	0.045	9.0±0.2	11000±500*
G76 -48	0.895	0.024	0.250	0.045	8.8±0.2	10200±500*

* Atmospheric parameters obtained with the diagram for T_{eff} < 12000 K, presented in Figure 6.

+ Atmospheric parameters obtained with Wehrse's models for log(g) = 8 according to Figure 7.

values have been included in Figures 5, 6, and 7. It
should be noted that for a given uncertainty of the
reddening-free colors the $\underline{w}$ versus $\underline{d}$ plane renders dif-
ferent uncertainties of the atmospheric parameters
depending on the convergency of the iso-gravity and iso-
temperature lines. Due to the fact that, in our approach,
the strength of H_β is the sole indicator of the gravity
the iso-gravity lines converge toward high and toward
low temperatures. In Figure 5 we have included points
for two very hot DA white dwarfs (EG 203 and EG 247) and
two DO stars (EG 86 and EG 71) in order to illustrate the
tendency of the iso-gravity lines. These four stars
also help to illustrate the small separation of the
iso-temperature lines above 30000 K.

Similar effects are apparent in Figures 6 and 7
where low temperatures are considered.

These properties of the $\underline{w}$ versus $\underline{d}$ plane hinder
attempts to extrapolate values of the atmospheric parame-
ter for those stars with observed reddening-free colors
falling outside the grid defined by the computed model
atmospheres. For this reason, the listed atmospheric
parameters (Table 9) of some very hot ($T_{eff} \geq 27000$ K)
stars are only estimates and no uncertainties are
attached.

Other Stars

The u, s, β, y photometry of non-DA stars (Table 5) was used to compute reddening-free colors and the results are presented in Table 10. Included in this set of stars is EG 283 (G 128-7), whose spectrum was classified as DAs,wk by Greenstein (1970), and later revised to DF, also by Greenstein (1975). For these stars, the w and d colors take values that are clearly out of the region defined by the grid of theoretical models and consequently, the derivation of gravity is not possible while the indicated temperature is rather uncertain.

In Figure 6 we have plotted the points corresponding to some stars that appear to have reddening-free colors somewhat similar to the black-body. We notice that the λ4135 star EG 129 (Grw + 70° 8247) has colors that indicate a temperature of about 18000 K. However, for this star the w and d colors are not good indicators of the temperature. Significant linear and circular polarization has been observed in EG 129 (Landstreet and Angel 1975) and the optical spectrum displays broad features that are very likely due to atomic helium. One of the absorption features is located near 4600 $\overset{\circ}{A}$, the region of our s photometric band; another absorption feature appears inside the region covered by the u photometric band. In the presence of these absorption

Table 10. Reddening-free indices for 16 non-DA white
dwarfs.

EG	Sp.T.	w	$\pm$m.e.	d	$\pm$m.e.
71	DO	1.011	0.024	-0.144	0.026
86	DO	1.003	0.065	-0.149	0.065
283	DF	1.034	0.015	0.275	0.047
54	DF	0.929	0.061	-0.417	0.048
329	DC,DF	1.010	0.034	-0.144	0.022
9	DC	0.980	0.039	0.045	0.062
52	DC	1.029	0.033	2.034	0.076
95	DC	1.019	0.026	0.643	0.053
148	DC	1.023	0.017	0.067	0.040
180	DC	1.042	0.041	0.121	0.047
202	DC	1.013	0.035	1.150	0.095
45	DK	1.159	0.024	1.609	0.045
129	λ4135	1.052	0.006	-0.038	0.014
250	DC	1.031	0.010	0.202	0.023
290	DAP	1.060	0.024	0.206	0.045
374	DXP	1.079	0.024	0.179	0.022

features the reddening-free color d becomes spuriously
small and indicates a larger temperature. According to
Wickramasinghe, Thompson and Strittmatter (1972), pure
helium atmospheres that approximate the observed spectrum
of EG 129 require an effective temperature of less than
12000 K.

Spectral features around 4600 Å have strong in-
fluence upon the determination of temperature due to the
fact that the magnitude measure with our s band enters
with weight 2.5, relative to the u and y bands, in the
d index. The effect is clearly observed in the DCP star
EG 374 (= G227-35). Greenstein (1974b) has observed an
absorption band, about 0.1 mag dip, centered at 4550 Å
in the spectrum of this star. The absorption feature
produces a redder (s-y) color that in turn reduces the
value of the d index. According to Figure 6, our obser-
vations indicate a temperature of about 7900 K for EG 374.
However, the color temperature, derived in the spectral
range between 3400 and 8000 Å, is only 7000 K
(Greenstein 1974b).

An interesting case is presented by the observa-
tions of the DAP star EG 290 (= G99-47). Low resolution
spectrum scans of this star show a smooth continuum that
is closely matched by a 5600 K black-body (Greenstein
1974b). However, the w and d colors indicate a

temperature of about 7000 K. Liebert, Dugel and Landstreet (1975) have obtained spectrum scanner observations with improved resolution (approximately 8 $\overset{\circ}{A}$) that confirm the smooth spectrum of EG 290 from 3900 to 7000 $\overset{\circ}{A}$, except for a weak absorption that appears to be consistent with the Zeeman pattern of H_α in a longitudinal magnetic field of few million gauss. Very broad and shallow features, commonly found in the spectra of polarized degenerate dwarfs, are not excluded, however, by the scanner observations (Liebert 1976). The similarity between the broad band colors of EG 290 and EG 283 (Greenstein, Gunn and Kristian 1971) is also found in the w versus d plane. The reddening-free colors of these two stars support the idea of almost equal effective temperatures; moreover, EG 283 is separated from the black-body line (in Figure 6) due to the effect of the weak H_β absorption in the w color.

In resume, the returns of our u, s, β, y photometry of non-DA degenerate stars are generally influenced by information of difficult interpretation. Therefore, unless significant a priori information on the spectral charactersitics is available, the u, s, β, y bands should not be used to derive atmospheric parameters of stars other than DA white dwarfs.

CHAPTER 5

INTERRELATIONS

The atmospheric parameters, derived in Chapter 4, are combined here with data on apparent magnitude, distance, and bolometric correction for a number of DA white dwarfs to investigate details in (a) the luminosity-temperature relation, and (b) the mass-radius-composition relation. Furthermore, the 46 stars with data in Table 9 provide a propitious sample to examine the number distribution with respect to effective temperature.

Effective Temperature Frequencies

The observed frequencies of effective temperature in DA white dwarfs gained in importance after Strittmatter and Wickramasinghe (1971) proposed the accretion-convection hypothesis of evolution. According to this hypothesis, a large portion of white dwarfs have helium-rich envelopes to which hydrogen, from interstellar material, is accreted. The DA spectrum of the white dwarfs is given by high temperatures and atmospheric layers in radiative equilibrium. As the stars cool, helium located in the inner layers begins to recombine

and significant convection takes place at $T_{eff} \approx 18000$ K.
According to the hypothesis convective transport modi-
fies the composition of the atmospheric layers and
changes the spectrum to DB type. Subsequent cooling
lowers the convection to deeper layers until it dis-
appears below the DB atmosphere at $T_{eff} \approx 15000$ K. Under
continuous accretion, the stars regain a DA spectral type
below 15000 K, when hydrogen remains on the surface.
Such an evolutionary picture implies a deficit of DA
white dwarfs in the temperature range that produces DB
spectral type. An analysis of UBV color indices provides
support for the hypothesis as stated by Strittmatter and
Wickramasinghe (1971). However, Shipman (1972) maintains
that effective temperatures derived through a match of
his model atmospheres with scanner observations, fail to
show a deficit of DA stars between 18000 and 15000 K.
It is interesting, therefore, to examine the distribution
of DA stars in terms of the temperatures derived with the
w̲ and d̲ indices.

Reliable effective temperatures have been de-
termined for 44 DA stars, according to the results in
Table 9. The data, grouped in bins of 1000 K that range
between 8500 and 27500 K, produce the histogram presented
in Figure 8. The number distribution is reduced to only
one star in the range 16500 K < T_{eff} < 18500 K, in sharp
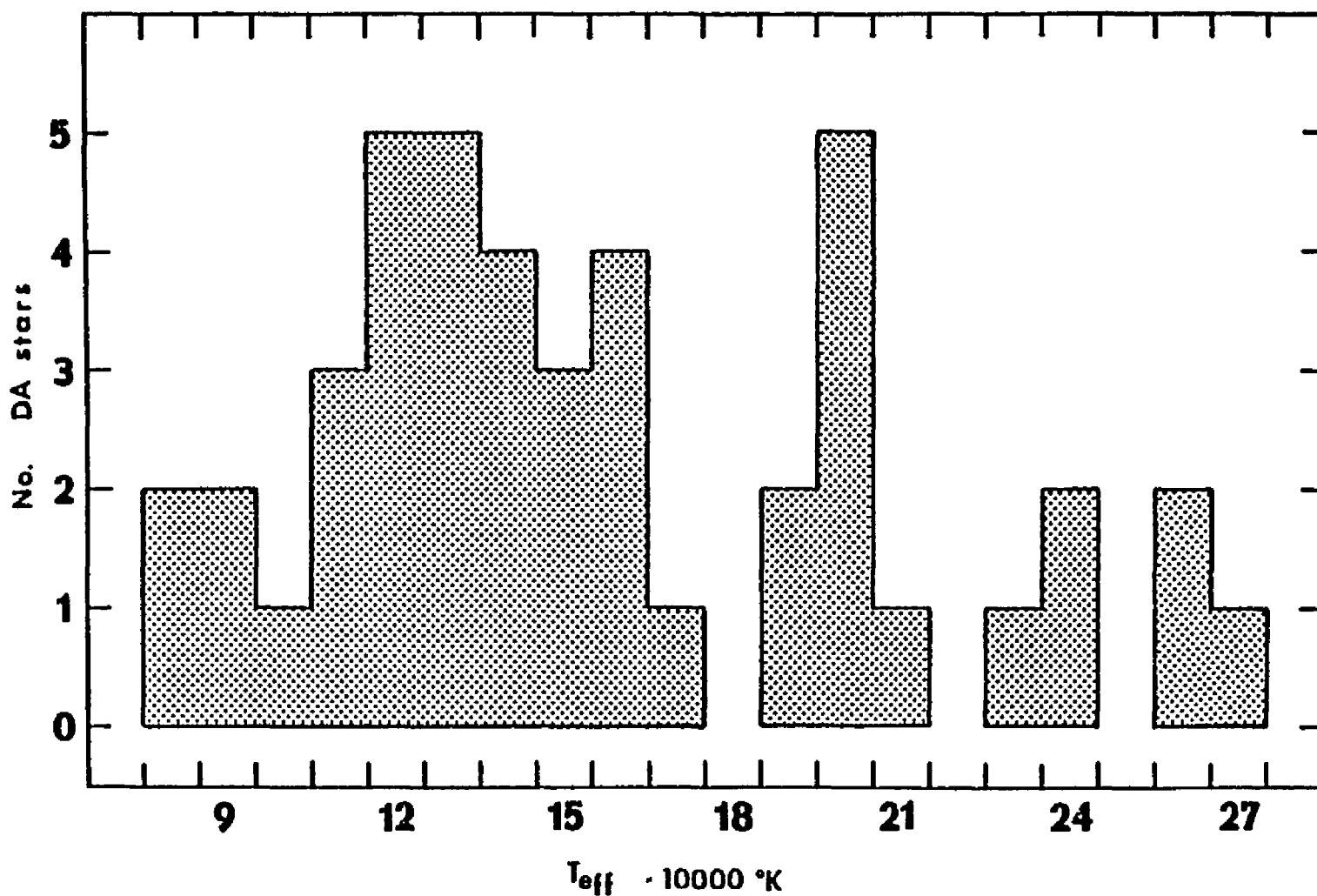
Figure 8. Effective temperatures histogram. -- The frequencies of effective
temperatures, derived with the $\underline{w}$ and $\underline{d}$ indices, for a group of
44 DA white dwarfs indicates a gap at 18000 K.

contrast with the adjacent ranges where frequencies of four or five stars are present. The small sample of DA white dwarfs available for this analysis is insufficient to derive conclusive results with a statistical test; however, it appears that there is a deficit of DA stars in approximately the same temperature range indicated by the UBV color indices. The clear exception is EG 150 with T_{eff} = 17000 ± 800 K. Four other stars, EG 33, 76, 83, and 161, populate the range 15500 K < T_{eff} < 16500 K. At the present time there are no reports of anomalies in the observed characteristics of these five stars. Nevertheless, it is interesting to notice that EG 33 and 83 are members of binary systems.

A comparison of our temperatures with the temperatures derived by Shipman (1972), for 15 stars in common, reveals that our determinations run generally lower by about 1000 K. The difference is very likely produced by the systematic error present in the absolute calibration employed to reduce the scanner observations (see Mihalas 1975). According to his data, Shipman (1972) finds six DA white dwarfs in the range 15000 K < T_{eff} < 18000 K. However, if an arbitrary correction of -1000 K is added to those temperatures, only two stars, viz. EG 29 and 33, remain in the same range.

Bolometric Magnitude-temperature Relation

An analysis of the H-R diagram, as traced by the data available to DA white dwarfs included in our sample, is presented in this section. For the abscissa of the H-R diagram we use here the logarithm of the effective temperature derived with the reddening-free indices. In a first approach to the luminosity, the absolute magnitude is used in the ordinate. The determination of absolute magnitudes is preceded by short reviews of the parallaxes and apparent magnitudes available for the stars in our sample. The information provided by the M_v versus $\log(T_{eff})$ diagram, and its comparison with early studies, leads to a consideration of the second approximation for the luminosity, namely the bolometric magnitude. This section is ended with the examination of the M_{bol} versus $\log(T_{eff})$ diagram.

Parallaxes

Twenty-eight DA white dwarfs listed in Table 11 have individual measurements of trigonometric parallax. Early measurements were obtained from the General Catalogue of Trigonometric Stellar Parallaxes (GCTSP) and its supplement (Jenkins 1952, 1963). More recent determinations were found in publications by Wagman (1967), Riddle (1970), van Altena (1971a, 1971b), Routly

Table 11. Trigonometric parallaxes.

EG No.	π_{abs}	$\pm$m.e.	Relative Values (x 0."001) and Weights
10	0."017	0."002	14N(40)
11	0.064	0.013	62C(6)
15	0.027	0.005	18A(20), 29N(40)
28	0.037	0.003	36N(40)
33	0.206	0.002	198A(20), 194C(7), 207M(10), 200Yk(10)
34	0.013	0.004	13N(40)
46	0.033	0.003	31.9S(40)
50	0.064	0.005	61M(8), 68N(40), 92St(3), 67V(7), 39W(7), 54Yk(10)
67	0.027	0.008	28N(40), 0V(10), 37W(7)
70	0.032	0.012	30A(7)
83	0.033	0.003	30N(40)
87	0.021	0.007	18N(20)
99	0.061	0.007	71C(7), 47M(4), 62N(40), 27Yk(6)
115	0.031	0.007	19A(28), 34N(40)
123	0.024	0.004	23N(30)
125	0.015	0.001	15A(20), 14N(40)
131	0.101	0.003	92A(20), 98N(40), 121Yk(10)
135	0.086	0.004	94A(20), 82N(40), 76W(7)
139	0.071	0.003	69A(40), 92M(70), 66N(40), 69S(40), 52W(16), 75Yk(8)
150	0.040	0.002	39N(40)
155	0.052	0.004	50N(40)
159	0.074	0.004	71N(40)
161	0.027	0.004	25N(40)
162	0.061	0.005	66A(20), 56N(40)
168	0.057	0.012	64N(40), 39Yk(20)
199	0.061	0.002	57N(40), 60.8Yk(35)
247	0.023	0.002	21N(40)
G76-48	0.041	0.005	39N(30)

(1972), Heintz (1973), Beardsley et al. (1973), Lippincott (1973), Thomas (1973), and Harrington et al. (1975). Parallaxes for EG 10, 87, 123, and G76-48 were kindly communicated, in advance of publication, by Dr. Conard C. Dahn (1976) of the Naval Observatory, Flagstaff station, Arizona.

For each star the collected relative parallaxes are listed in the fourth column of Table 11. The source of individual values is indicated by the usual observatory abbreviations, and the corresponding weight is given in parenthesis. Parallaxes found in the GCTSP retain the weight given there. For parallaxes given in other publications the general precepts for weight computation described in the GCTSP were used, except that the uncertainties were not adjusted as recommended by Jenkins (1952). This procedure could produce a weighted average slightly biased toward the more recent determinations of the parallax. Nevertheless, modern measurements of trigonometric parallax have more than twice the accuracy of the parallaxes compiled in the GCTSP at the end of 1962, and preference for the newer determinations is desirable.

The weighted average of the relative parallaxes was reduced to absolute and presented in the second column of Table 11. Corrections from relative to absolute

parallax were interpolated from the mean parallaxes computed by van Altena (1974). The third column of Table 11 presents the mean errors of the average relative parallax.

Seven white dwarfs in our program are highly probably Hyades cluster members. Unfortunately, no individual parallaxes have been measured for any of these stars. Upgren (1974) and Klemola et al. (1975) have determined an accurate mean parallax for the cluster. The results are 0."0219 ± 0."0018 (m.e.) and 0."0230 ± 0."0015 (m.e.), respectively. However, the distance modulus appear to be known with better accuracy. Hanson (1975) derived a mean distance modulus for the Hyades cluster of 3.29 ± 0.08 mag. For the seven white dwarfs mentioned above we adopt here 3.29 ± 0.20 mag, where the uncertainty is consistent with the mean error of the cluster's mean parallax.

Apparent Magnitudes

Visual magnitudes of the white dwarfs in our program have been obtained by numerous observers. A compilation of all the published results would include early observations with unknown accuracy and poorly defined photometric bands. In order to derive more accurate V magnitudes we have decided to compile the results of only homogeneous systems with observations of

a significant number of DA white dwarfs. Accordingly, we selected the photometry obtained by Eggen and Greenstein (1965a), the results of Graham (1972), and the photometry carried out at the Naval Observatory (Harrington et al. 1975). A list of these results is presented in Appendix B. The V magnitude of those four systems has been combined with our data presented in Table 4 to produce a weighted average, where the weight is given by the number of observations in the respective systems. This average contains a degree of uncertainty that represents the external errors in photoelectric photometry. From our discussion in Chapter 3 we estimate that uncertainty at 0.04 mag.

M_V versus $\log(T_{eff})$

In order to facilitate the analysis the stars with measured trigonometric parallax and good determination of the effective temperature have been listed in Table 12. The second column presents the absolute magnitude $M_V = V + 5 + 5 \log(\pi_{abs})$. The third column presents the uncertainty of M_V computed with the relation $\sigma = \sqrt{\sigma_V^2 + \sigma_\pi^2}$, where σ_V is the uncertainty of the apparent magnitude and $\sigma_\pi = 5 \times \log(e) \times [\text{relative error of } \pi_{abs}]$. Because in general $\sigma_\pi > \sigma_V$ the uncertainty of M_V is given mainly by σ_π. The next two columns present the values

Table 12. Variables for the H-R diagram.

EG No.	M_V mag	σ mag	$\log(T_{eff})$	σ	B.C. mag	M_{bol} mag
10	10.32	0.25	4.08	0.04	-0.70	9.62
11	11.87	0.44	3.90	0.02	-0.40	11.47
15	10.38	0.40	4.20	0.02	-0.75	8.63
26H	11.18	0.18	4.13	0.01	-0.93	10.25
28	11.63	0.18	4.18	0.01	-1.15	10.48
29H	11.99	0.18	4.18	0.01	-1.15	10.84
33	11.04	0.03	4.19	0.04	-1.23	9.81
34	11.18	0.67	4.15	0.01	-1.00	10.81
36H	10.99	0.18	4.29	0.02	-1.90	9.09
37H	10.73	0.18	4.35	0.02	-2.13	8.60
38H	10.62	0.18	4.41	0.02	-2.55	8.07
39H	10.86	0.18	4.31	0.01	-1.90	8.96
42H	10.54	0.18	4.44	0.03	-2.65	7.89
46	11.06	0.20	4.42	0.03	-2.58	8.48
50	11.03	0.17	4.30	0.02	-1.90	9.13
67	10.46	0.64	4.12	0.01	-0.85	9.61
70	10.52	0.81	4.38	0.03	-2.32	8.20
83	11.24	0.20	4.20	0.01	-1.29	9.95
87	9.86	0.72	4.08	0.02	-0.79	9.07
99	11.25	0.25	4.15	0.02	-1.00	10.25

Table 12. -- <u>Continued</u>.

EG No.	M_V mag	σ mag	$\log(T_{eff})$	σ	B.C. mag	M_{bol} mag
115	11.82	0.49	4.05	0.01	-0.58	11.24
123	11.26	0.36	4.10	0.01	-0.78	10.48
125	9.80	0.14	4.11	0.01	-0.81	8.99
131	12.29	0.06	4.18	0.01	-1.15	11.14
135	13.34	0.10	3.95	0.05	-0.45	12.89
139	10.80	0.09	4.28	0.02	-1.75	9.05
150	10.80	0.11	4.23	0.02	-1.45	9.35
155	12.92	0.17	4.04	0.04	-0.60	12.32
159	12.37	0.12	4.08	0.02	-0.70	11.67
161	12.48	0.32	4.20	0.02	-1.30	11.18
162	11.86	0.18	4.15	0.02	-1.00	10.86
168	13.28	0.46	3.90	0.03	-0.40	12.68
199	13.29	0.07	3.93	0.02	-0.42	12.87
G76-48	14.02	0.26	4.01	0.02	-0.67	13.35

of $\log(T_{eff})$ and the respective uncertainty given by

$\sigma = \log(e) \times$ [relative error of T_{eff}].

Those DA white dwarfs for which modern determination of the parallax indicate $\pi \geq 0."025$ have been included in the M_V versus $\log(T_{eff})$ diagram presented in Figure 9. This condition excludes EG 11 for which only one early determination is available. Nine stars for which $\pi_{abs} \geq 0."060$ are presented with circles. Squares are used for the seven Hyades white dwarfs. As indicated by the dotted lines in Figure 9, the distribution of the points appears to define two sequences. In the upper sequence, containing six Hyades white dwarfs, the dotted line represents the relation

$$M_V = 20.75 - 2.3 \log(T_{eff}) \ . \qquad (19)$$

Aside from the smaller number of stars considered, Figure 9 bears a strong resemblance with the M_V versus (U-V) diagram obtained by Eggen and Greenstein (1965a in Figure 4 of their work, p. 95). The upper sequence derived by these authors is well represented by the relation

$$M_V = 11.65 + 0.85 \ (U-V) \qquad (20)$$
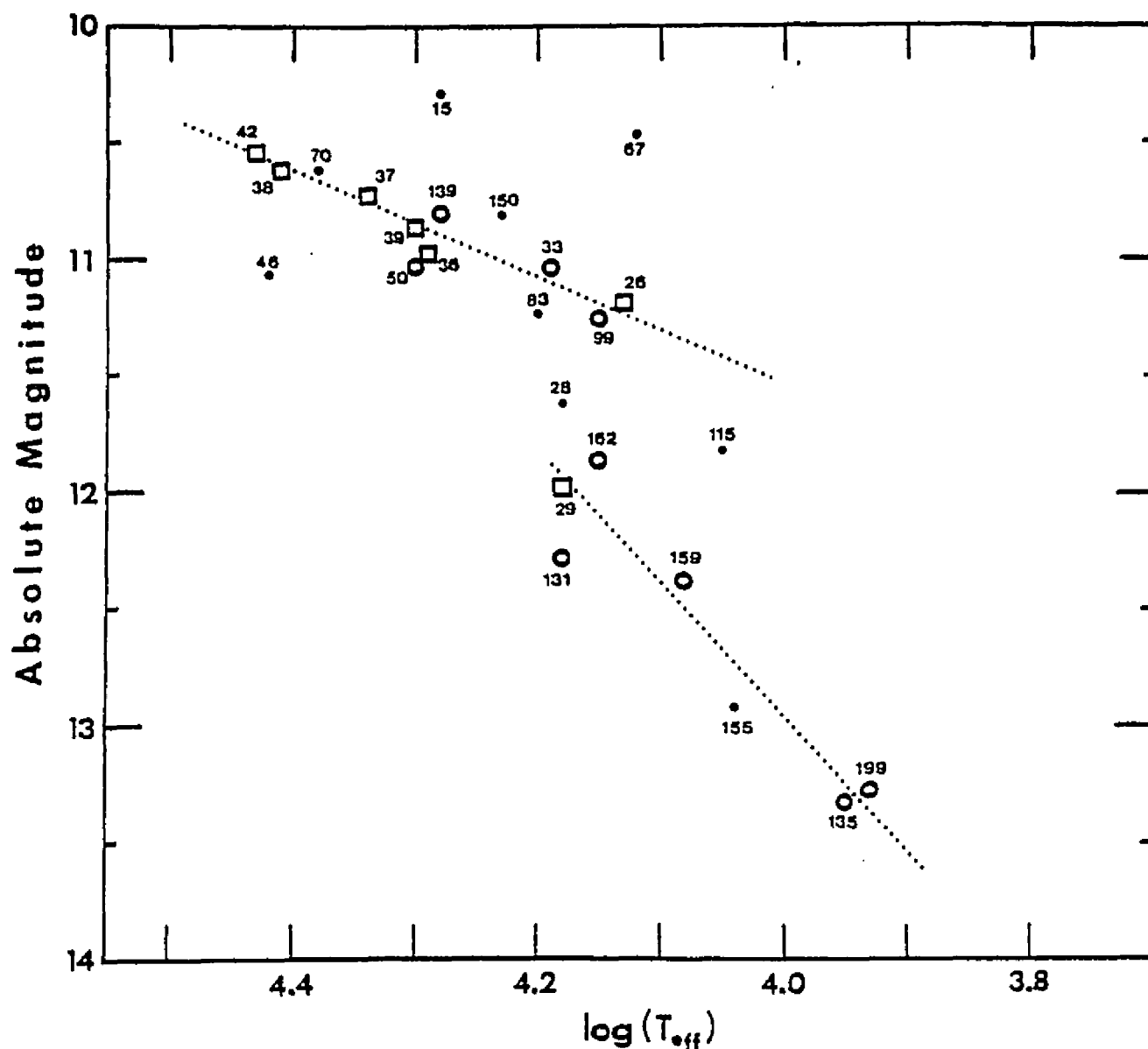
Figure 9. The M_V versus $\log(T_{eff})$ diagram for DA white dwarfs. — Data for stars with $\pi \geq 0.''025$ and Hyades members is presented. Only stars with $\pi \geq 0.''06$ (presented with circles) and Hyades members (with squares) were used to derive the slope of the dotted lines. Except for EG 15, 67, and 80, the stars included in the diagram have absolute magnitude uncertainty equal or lower than 0.25 mag.

corresponding to a set of about 20 degenerate stars hav-
ing (U-V) between -0.9 and 0.0 mag. An inventory of
these stars reveals that most of the DA white dwarfs
used to derive Equation 20 were also used to
derive Equation 19. Therefore, the clear match
between both diagrams cannot be considered unex-
pected.

There is, however, a net contribution. Elimina-
tion of the absolute magnitude between both relations
renders an independent calibration of the effective
temperature in terms of the (U-V) color, for the stars
in the upper sequence. The result can be expressed as

$$(U-V) = 2.7 \log(\theta) + 0.68 \qquad (21)$$

where the reciprocal temperature, $\theta = 5040/T_{eff}$, is used
for purpose of comparison with the calibrations compiled
by Shipman (1972, in Figure 4 of his work, p. 735). In
the range $0.18 \leq \theta \leq 0.35$, corresponding to the range
of $\log(T_{eff})$ where the upper sequence is well defined in
Figure 9, this new calibration runs between Shipman's
own calibration and the original calibration by Terashita
and Matsushima (1969). The implications of this agree-
ment will be discussed in the next chapter.

We now turn to the lower sequence that is indicated in our Figure 9 and in the M_V versus (U-V) diagram of Eggen and Greenstein (1965a). Relations of the type described above are not available in this case, mainly because the lower sequence found by Eggen and Greenstein contains a dispersion too large for deriving a linear relationship. Such dispersion is sufficiently small, however, to establish a clear separation from the upper sequence. In the case of our data, the lower sequence appears better defined although it depends on only seven stars with accurate absolute magnitude. Two characteristics of the lower sequence, first pointed out by Eggen and Greenstein (1965a), come in sight also on our data. They are: steeper slope and fainter zero point than the upper sequence. The fact that these two characteristics prevail in the dependence of M_V in terms of (U-V) and in terms of $\log(T_{eff})$ suggest that a temperature calibration, similar to Equation 21 is also possible for a lower sequence. Actually, cursory examination of both diagrams indicates that, within the uncertainty of both sets of data, the relation

$$(U-V) \simeq 2.7 \log(T_{eff}) + 0.3 \qquad (22)$$

provides a satisfactory first approximation for the required temperature calibration. Implicit in this relation is the assumption that observational errors produce the

dispersion observed in the lower sequence of the M_v
versus (U-V) diagram. If such dispersion is an intrinsic
characteristic of the stars, the last term in Equation 22
should be a variable in the range between 0.2 and 0.6
mag.

Independent of this uncertainty, the comparison
of the M_v versus (U-V) diagram derived by Eggen and
Greenstein (1965a) and the M_v versus $\log(T_{eff})$ diagram
presented in Figure 9 provides substantial support for
the existence of a second sequence of degenerate stars.

M_{bol} versus $\log(T_{eff})$

Adding the bolometric corrections to the absolute
magnitudes produces a homologous transformation of these
two sequences into the M_{bol} versus $\log(T_{eff})$ diagram.
The bolometric corrections, derived by interpolation in
the tables published by Strittmatter and Wickramasinghe
(1971), are listed in Table 12. The results are illus-
trated in Figure 10, where nine stars with parallax
$\pi \geq 0."06$ and seven Hyades members are included. The two
sequences appear to have similar slope in the M_{bol} versus
$\log(T_{eff})$ presented in Figure 10. For these 16 stars
the bolometric magnitude is known with uncertainty
equal or smaller than 0.2 mag. Although the two sequences
are still indicated when all the stars used in Figure 9
are included, only the stars with high quality
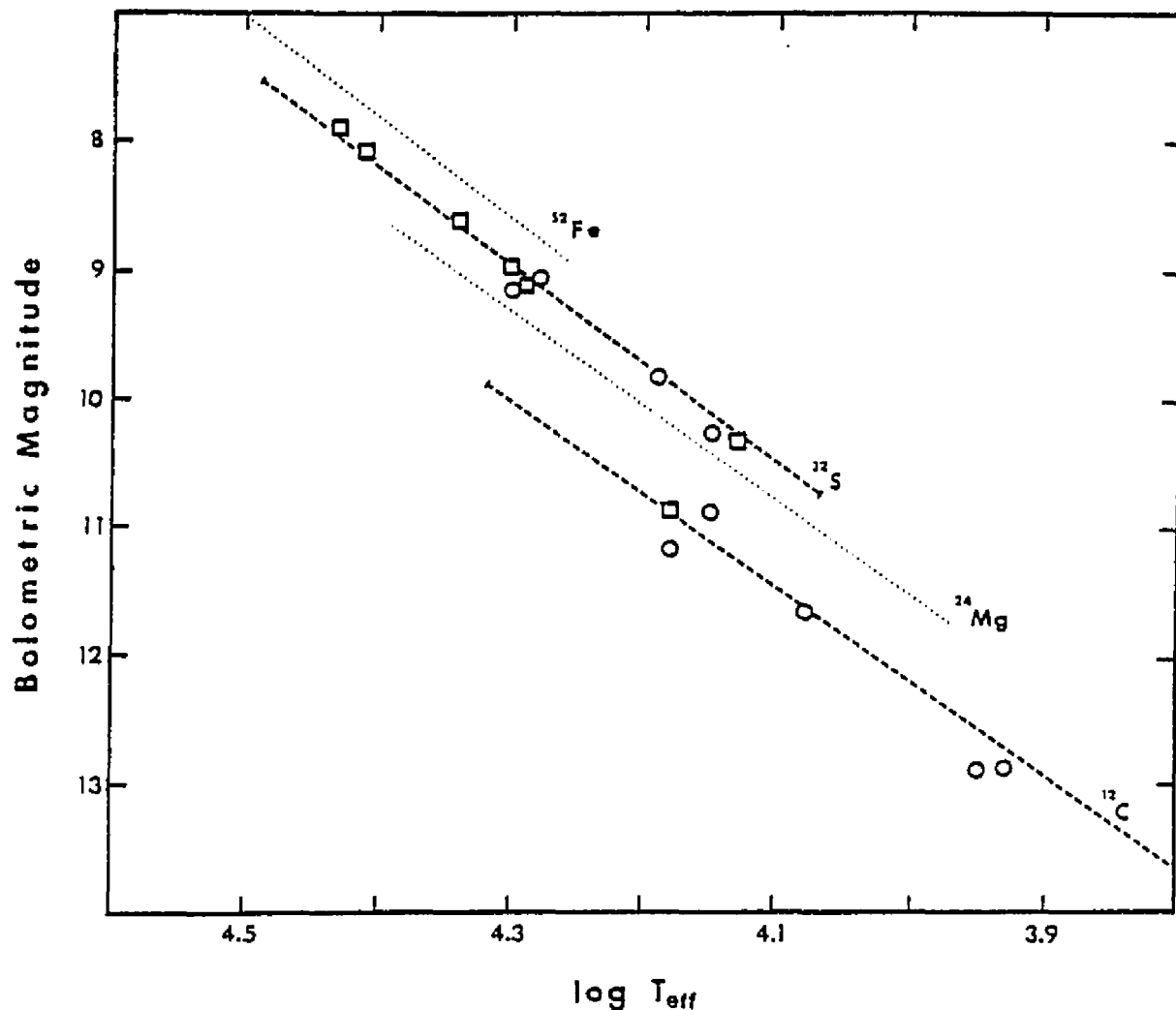
Figure 10. The M_{bol} versus $\log(T_{eff})$ diagram for DA
white dwarfs. — Data from 16 stars with
trigonometric parallax $\pi > 0.''06$ plus
Hyades members have been plotted with the
symbols as in Figure 9. For comparison, the
crystallization sequences computed by Van
Horn (1968) have been plotted with dashed and
dotted lines. As presented here, the ^{32}S and
^{24}Mg sequences are restricted to degenerate
dwarfs in the $0.88 \leq M/M_O \leq 0.40$ range, with
the larger mass at the upper end.

bolometric magnitude have been retained in Figure 10
because they present a closer alignment without excep-
tion. The similarity with Figure 9 allows an easy
identification of the EG numbers for these 16 stars.
For purpose of reference four crystallization sequences,
theoretically derived by Van Horn (1968), have been out-
lined on the same diagram. The upper observational
sequence is defined by ten DA white dwarfs, six of them
members of the Hyades cluster. Only six stars define
the lower observational sequence. The apparent coinci-
dence of the two observational sequences with the ^{12}C
and ^{32}S crystallizationsequences is not surprising,
however. It was noticed first by Van Horn (1968) in his
analysis of the UBV photometry of degenerate dwarfs
published by Eggen and Greenstein (1965a).

In terms of the uncertainties of the bolometric
magnitudes, the separation of the two sequences in
Figure 10 is well established. The uncertainty reaches
0.25 mag for only one star (EG 99 at M_{bol} = 10.25,
$\log(T_{eff})$ = 4.15). The 15 DA white dwarfs remaining
have uncertainties equal to or smaller than 0.18 mag.

Although identification of the observational data
with the ^{12}C and/or ^{32}S sequences is not straightforward,
the results presented in Figure 10 lend strong support

to the suggestion that cooling white dwarfs proceed along more than one crystallization sequence.

Mass-radius Relation

In the original sample of DA white dwarfs observed with the u, s, β, and y bands there are 34 stars for which, aside from $\log(T_{eff})$ and $\log(g)$, the bolometric magnitude is also available. For this subset of stars, listed in Table 12, the respective radius and mass was derived. Computation of the radius was made with the relation

$$\log\left(\frac{R}{R_o}\right) = -2 \log(T_{eff}) - 0.2\ M_{bol} + \frac{42.36}{5}$$

(23)

and the result is presented in Table 13. Analytic propagation of the errors (listed in Table 12) was employed to derive the uncertainty of the computed radii.

Similarly, determination of the mass was obtained with the relation

$$\log\left(\frac{M}{M_o}\right) = 2 \log\left(\frac{R}{R_o}\right) + \log\left(\frac{g}{g_o}\right),$$

(24)

and the results, together with the propagated errors, are presented in Table 13.

Table 13. Radius, gravity, and mass for selected DA white dwarfs.

EG No.	$\log(R/R_O)$	σ	$\log(g)$	σ	$\log(M/M_O)$	σ
10	-1.61	0.09	8.0	0.2	+0.34	0.27
11	-1.63	0.10	8.0	0.2	+0.30	0.28
15	-1.81	0.08	8.0	0.2	-0.06	0.26
26	-1.84	0.04	7.8	0.1	-0.32	0.13
28	-1.98	0.05	7.9	0.1	-0.49	0.50
29	-2.05	0.05	8.1	0.2	-0.43	0.22
33	-1.87	0.08	7.7	0.1	-0.48	0.19
34	-1.98	0.14	7.0	0.4	-1.40	0.49
36	-1.93	0.05	8.1	0.2	-0.21	0.22
37	-1.95	0.05	9.0	0.2	+0.66	0.22
38	-1.97	0.05	9.2	0.2	+0.82	0.22
39	-1.95	0.05	7.5	0.3	-0.83	0.32
42	-1.98	0.07	8.3	0.6	-0.09	0.62
46	-2.07	0.08	8.4	0.4	-0.17	0.43
50	-1.96	0.05	8.1	0.1	-0.26	0.14
67	-1.68	0.13	7.3	0.1	-0.51	0.28
70	-1.93	0.17	8.2	0.3	-0.09	0.45
83	-1.93	0.05	7.6	0.2	-0.69	0.22
87	-1.49	0.15	8.9	0.2	+1.48	0.36
99	-1.88	0.07	7.7	0.2	-0.49	0.24

Table 13. -- <u>Continued</u>.

EG No.	$\log(R/R_\odot)$	σ	$\log(g)$	σ	$\log(M/M_\odot)$	σ
115	-1.88	0.10	7.7	0.2	-0.50	0.28
123	-1.83	0.07	7.4	0.1	-0.70	0.17
125	-1.55	0.04	7.1	0.2	-0.44	0.21
131	-2.11	0.03	...	...	...	...
135	-2.01	0.10	8.5	0.4	$+0.03$	0.45
139	-1.89	0.05	7.8	0.3	-0.43	0.32
150	-1.86	0.05	7.9	0.4	-0.26	0.41
155	-2.07	0.09	8.3	0.5	-0.29	0.53
159	-2.01	0.05	8.0	0.1	-0.46	0.14
161	-2.17	0.07	8.6	0.1	-0.18	0.17
162	-1.99	0.05	7.8	0.2	-0.62	0.22
168	-1.87	0.11	8.0	0.2	-0.18	0.30
199	-1.96	0.04	8.5	0.4	$+0.15$	0.41
G76 -48	-2.21	0.06	8.8	0.2	-0.06	0.23

For a majority of the stars included in Table 13 the uncertainty in the logarithm of the mass is less than 0.50, indicating a relative improvement with respect to earlier mass determinations. Stars for which uncertainty in the logarithm of the mass is less than 0.30 have been included in the mass-radius diagram presented in Figure 11. Two stars with accurate determinations of the mass due to their binary character (40 Eri B and Sirius B) are shown with error bars.

The resulting mass-radius diagram displays two main characteristics: (1) the DA white dwarfs appear to follow the theoretical mass-radius relation as derived by Hamada and Salpeter (1961) for heavy metals, and (2) there is a significant concentration of stars in the range $0.16 \leq M/M_o \leq 0.98$.

Four stars (EG 10, 11, 37 and 38) appear to follow the mass-radius relation for pure hydrogen internal composition. An attempt to explain the location of these stars in terms of anomolous characteristics has been partially successful in the case of EG 11 only. The absolute luminosity determination of EG 11 is based on one measurement of the trigonometric parallax, with relatively large error (see Table 11). For a DA white dwarf with effective temperature near 7900 K,

Figure 11.   The mass-radius diagram. -- The masses and radii obtained in this
             chapter are plotted for DA white dwarfs. Circles are used to
             represent the data with uncertainty < 0.2 in the logarithm of the
             mass. Triangles represent stars where the uncertainty ranges
             between 0.2 and 0.3. The crosses correspond to 40 Eri B and Serius
             B, with masses derived from their respective binary orbits.
             Theoretical curves are due to Chandrasekhar (1939) (H) and
             to Hamada and Salpeter (1961) (Mg, Fe). The lower curve, without
             label, is the mass radius relation for stars with neutron core
             as given by Hamada and Salpeter (1961).
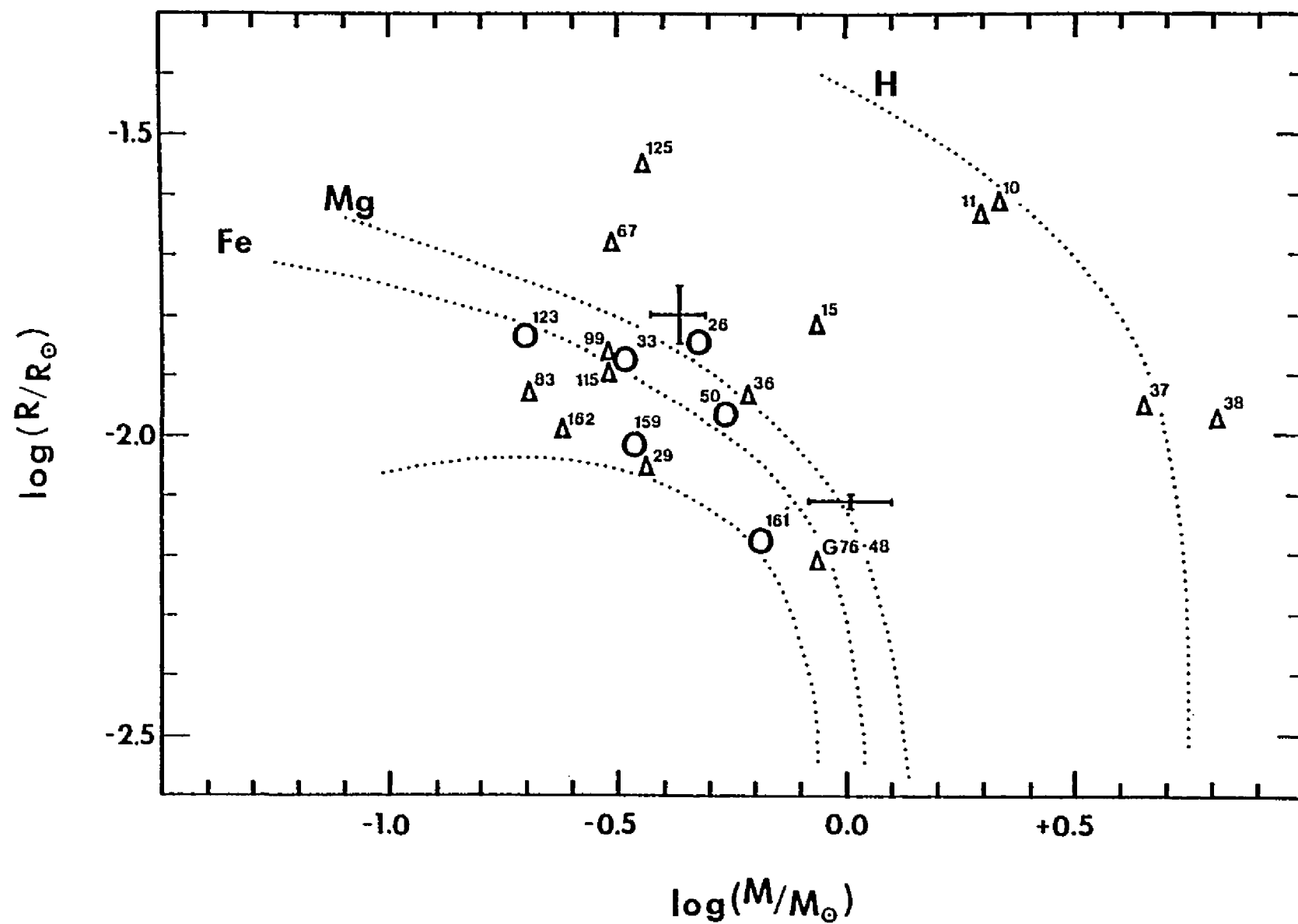
Figure 11. The mass-radius diagram.

the absolute magnitude of EG 11 is too bright, as indicated by other white dwarfs with similar temperatures.

Further investigations of EG 10, 11, 37 and 38 are required before their location in the mass-radius diagram can be established conclusively.

CHAPTER 6

DISCUSSION AND CONCLUSIONS

The analysis contained in the previous chapter
indicates that the temperatures derived in this investi-
gation lend support to two results already known from
UBV colors as temperature indicators. These results are:
(1) the reduced number of DA white dwarfs with T_{eff} be-
tween 16000 K and 18000 K detected by Strittmatter and
Wickramasinghe (1971) and (2) the two sequences in the
H-R diagram found by Eggen and Greenstein (1965a).
Corroboration of these results with the u, s, β and y
bands may appear surprising in first instance since
elaborate analysis of the UBV colors of DA white dwarfs
indicates that atmospheric parameters derived with these
broad bands are unreliable (Weidemann 1975). However,
we have also found that there is an accurate linear rela-
tion (see Equation 16) between the (U-V) color and the
effective temperatures derived fromthe w̲ versus d̲ plane.
Such a result can be anticipated because a comparison
between the Paschen and Balmer continua (although mea-
sured with the U and V bands) is necessarily dependent

on the temperature. Furthermore, the compilation of effective temperature calibrations published by Shipman (1972) indicates that the dependence of (U-V) on the temperature is very strong in the 14000 K $\leq T_{eff} \leq$ 28000 K range.

Here we discuss the two results referred to above under the assumptionthat the scale of temperature derived with both photometric systems represents adequately the actual temperatures of DA white dwarfs.

Let us consider first the deficiency in the number of DA white dwarfs observed at effective temperatures between 16000 K and 18000 K. As indicated in Chapter 5, an arbitrary correction of -1000 K in the scale of temperatures derived by Shipman (1972) reveals that only two stars of his sample populate the mentioned range. Instead of contradicting the results of this work, or the data analyzed by Strittmatter and Wickramasinghe (1971), Shipman's (1972) result points to some uncertainty in the zero point of the temperature calibrations. Independent of such uncertainty, the three results appear to be consistent with the accretion-convection hypothesis invoked by Strittmatter and Wickramasinghe (1971) to account for the existence of the pure helium atmosphere, DB white dwarfs.

The main drawback of these three results is the
small statistical sample of DA white dwarfs included in
each instance. It may be that the shortage of DAs is
only a statistical fluctuation in such a small sample.
Sion and Liebert (1977) have examined a sample of 424
spectroscopically identified white dwarfs and find no
apparent deficiency in the number of DAs in the interval
of absolute magnitude populated by most of the DB stars.
This result seems to be in agreement with the quantita-
tive analysis of the accretion-convection hypothesis
carried out by D'Antona and Mazzitelli (1975) which indi-
cates that the difference between DA and DB atmospheres
cannot be due to accretion and mixing processes only,
and that for high effective temperatures the existence
of accretion is questionable. However, the final word
on these matters has not been written. The most recent
contribution to this problem is some empirical evidence
that mixed atmospheres exist: Wickramasinghe and Whelan
(1977) have discovered that weak hydrogen lines are
observed in the spectrum of the helium rich (spectral
type DB) white dwarf EG 153. Estimated relative abun-
dances give a helium to hydrogen ratio between 10^4 and 10^5,
and the effective temperature appears to be in the range
between 15000 K and 20000 K. Further study of EG 153,
and perhaps the discovery of other similar stars, may

provide some conclusive evidence on the role of accretion in the evolution of white dwarfs.

Let us examine now the two sequences observed on the H-R diagram. The origin of the controversy over the existence of two observational sequences for degenerate dwarfs can be traced to the single band apparent in the M_V versus (b-y), i.e., the H-R diagram in terms of the Stromgren color used by Graham (1972). The discrepancy between this single band and the two bands evident in the M_V versus (U-V) diagram (Eggen and Greenstein 1965a) is far too great to be attributed to observational errors, as indicated by Eggen (1969). However, it has been shown in this work that the (b-y) color is not a good temperature indicator due to contamination by the board absorption of H_β. Furthermore, the slope of the Paschen continuum becomes less and less sensitive to temperatures above 10000 K. A better temperature indicator for DA white dwarfs should be the Stromgren (u-y) color, for the same reason that the Johnson (U-V) color is a good temperature indicator. Due to the large difference between the Paschen and Balmer continua near the Balmer jump one can predict that even the (u-b) color is a better temperature indicator than (b-y). In effect, a plot of M_V versus (u-b) with the data published by Graham (1972) reveals two clear bands

resembling the results obtained by Eggen and Greenstein (1965a) and Figure 9 of this work. The M_v versus (u-b) diagram obtained with Graham's data is presented in Appendix C. It appears, therefore, that the two bands of degenerate dwarfs on the H-R diagram have been observed by three independent photometric systems.

The brightness along the crystallization sequences is strongly dependent on the mass of the stars. More massive degenerate dwarfs should populate the brighter end of each individual sequence, with a monotonic decrease of the mass toward the faint end. In Figure 10 the theoretical sequences corresponding to ^{24}Mg and ^{32}S have been drawn for the mass range $0.88 \leq M/M_o \leq 0.40$. The faint ends of these sequences outline the slope of lines of equal mass. The steeper slope corresponding to the lines of equal mass indicates that at a given effective temperature only a small section of the crystallization sequences will overlap if the masses of most white dwarfs are concentrated in a narrow mass range. The small overlap of the ^{12}C and ^{32}S sequences is clearly observed in Figure 10. This result is consistent with the narrow range of masses ($0.16 \leq M/M_o \leq 0.98$) for most of the white dwarfs included in the mass-radius diagram presented in Figure 11.

Variations of the mass for the stars along the bright sequence, presented in Figure 10, can be examined in Table 14. The theoretical mass is listed in the second column. This is the mass corresponding to each of the ten stars after interpolation from Van Horn's (1968) model (see Table 1 of his paper, p. 231) and scaled to the crystallization sequence of ^{32}S white dwarfs. The mass determined in this work using Equation 19 is listed in the third column. The gravity and relative radii, also reproduced from Table 13 in Chapter 5, are listed in the fourth and fifth columns, respectively.

Within the uncertainty of 1σ five stars (EG 42, 50, 36, 139 and 26) agree with the theoretical mass. Two more stars (EG 33 and 99) also follow the monotonic variation of the mass if the acceptable level of un-certainty is raised to 2σ. According to the comparison between theoretical and empirical masses it is clear that the observational results are not in contradiction with the hypothesis for crystallization sequences. The large uncertainties in the empirical masses of EG 37 and 38 make their comparisons with the theoretical values inconclusive. Only in the case of EG 39 is there a clear discrepancy with the theoretical mass.

The evident separation of the two observational sequences and their coincidence with the ^{32}S and ^{12}C

Table 14. Variables of the brighter crystallization
           sequence.

Theoretical		Empirical		
EG No.	M/M_o	M/M_o	g	$\log(R/R_o)$
42	0.88	0.81±1.16	2.0×10^8	-1.98±0.07
38	0.81	6.61±3.35	15.8	-1.97±0.05
37	0.71	4.57±2.32	10.0	-1.95±0.05
39	0.66	0.15±0.11	0.9	-1.95±0.05
50	0.65	0.55±0.18	1.3	-1.96±0.05
36	0.64	0.62±0.31	1.3	-1.93±0.05
139	0.63	0.37±0.27	0.6	-1.89±0.05
33	0.60	0.33±0.14	0.5	-1.87±0.08
99	0.56	0.32±0.18	0.5	-1.88±0.07
26	0.45	0.48±0.14	0.6	-1.84±0.04

crystallization sequences raises two questions. First, is it possible that during pre-white dwarf evolution nucleosynthesis can reach the formation of ^{32}S? And second, what is the reason for a dichotomy in the final composition of the white dwarfs? To the extent that parent stars of white dwarfs should have a moderate mass, with an upper limit of ~5 M_o according to Weidemann (1977), nuclear processing will not reach such heavy nuclei as suggested by current trends in nucleosynthesis research. Nevertheless, assuming that white dwarfs with nuclei as heavy as ^{32}S originate in some massive stars or they are formed in highly evolved binaries, after several stages of mass transfer, one would expect to observe intermediate crystallization sequences, not only the ^{12}C and ^{32}S sequences.

A satisfactory answer to these questions appears to be the effect of crystallization and variation of specific heat upon the probability of observing a white dwarf of a given mass and chemical composition in the interval $\Delta \log(L/Lo)$ as studied by Van Horn (1968). In the case of white dwarfs consisting of ^{12}C, values of high probability density define two separate areas on the H-R diagram coinciding in extention and slope with the two observational sequences. The area located on the brighter sequence arises from the higher probability

corresponding to more luminous white dwarfs. The other
area of high probability density, coincident with the
fainter sequence, results from the onset of crystalliza-
tion in ^{12}C white dwarfs. This is an attractive inter-
pretation of the two sequences in the H-R diagram because
it eliminates the need for degenerate dwarfs composed
of elements much heavier than oxygen and/or carbon.
This interpretation also accounts for the lower number
of DAs observed in the lower sequence.

Van Horn (1977) has pointed out that, according
to the improved calculations reported by Lamb and Van
Horn (1975), at the onset of crystallization a 1 M_o,
pure ^{12}C white dwarf should appear at M_{bol} = 11.69 and
$\log(T_{eff})$ = 4.120 on the H-R diagram. By the time that
half of the mass is crystallized the position has shifted
to M_{bol} = 12.74 and $\log(T_{eff})$ = 4.015. These values
indicate that the theoretical crystallization sequence
for carbon white dwarfs is actually lower by $M_{bol} \simeq 0.4$
to 0.5 mag than the ^{12}C sequence of the original computa-
tions (Van Horn 1968). This new result indicates that
the coincidence between the observational data and the
theoretical sequence is also produced by other effects
aside from crystallization. Van Horn (1977) has suggested
two other effects. First, the increase in luminosity
by different atmospheric opacities, and second, the

brighter crystallization sequences expected in a carbon core, hydrogen envelope white dwarfs. This second suggestion is based on the calculations by Fontaine and Van Horn (1967) indicating that white dwarf models with a hydrogen envelope display brighter luminosity ($M_{bol} \simeq -0.6$ to -1.0 mag near $10 \leq M_{bol} \leq 12$ mag) than pure carbon models. The following steps into the understanding of the sequences may be the theoretical determination of the thickness of a hydrogen envelope and the percentage of crystallized mass that are required to match the observational data.

Finally, let us consider the traditional test for the theory of degenerate dwarfs: the mass radius diagram. To the extent that the models of degenerate dwarfs, with homogeneous composition, can be parameterized in terms of the mean molecular weight per electron, there is a one-to-one relation between the mass and the radius. In the framework of this theory the composition of the thin, non-degenerate atmosphere has no influence in the determination of the radius or the mass. Accordingly, DA atmospheres are masking an internal composition of heavier elements. At the present time, empirical and theoretical determinations of the mass and the radius have insufficient accuracy to survey such internal compositions. The present consensus, however, is that

there is no serious discrepancy between theory and ob-
servations. Weidemann (1971) and Wickramasinghe and
Strittmatter (1972) have pointed out that the major
source of uncertainty in the determination of masses and
radii comes from the uncertainty in the distance to the
white dwarfs. Due to this uncertainty the empirical
data will show larger scatter in a direction almost per-
pendicular to the theoretical mass-radius relations for
different compositions. The advent of new, more accurate,
parallax determinations have reduced some of the scatter,
as indicated by Figure 11 at least for DA white dwarfs.
A comparison of Figure 11 with the mass-radius diagram
derived by Wickramasinghe and Strittmatter (1972), based
mainly in old parallax determinations, indicates that bhe
new data is in better agreement with the mass-radius re-
lations computed by Hamada and Salpeter (1961).

Nevertheless, it remains to investigate the
nature of the large masses derived for EG 37 and 38 (see
Figure 11 and Table 14). Such large masses become a
source of doubt on the degenerate-dwarf character of both
stars. However, the spectroscopic analysis of these two
stars is unequivocal on the effects of high surface
gravity upon the absorption lines of hydrogen (Eggen and
Greenstein 1965a). According to those observations both
stars are bona fide white dwarfs. It is possible then

that in the case of these two stars, the masses derived here are affected by a systematic error. The analysis of the uncertainty attached to the value of $\log (M/M_o)$ quoted in Table 13 indicates that such systematic error is plausible. In the cases of these two stars the uncertainty of $\log (M/M_o)$ amounts to 0.22 in the logarithm, a value that is comparable with the uncertainty of several other DA white dwarfs with masses about 0.3 M_o. Consequently the large masses arise from an error in some term of Equation 23 and Equation 24. Examination of the values of $\log(T_{eff})$, $\log(g)$ and their respective uncertainties (see Table 13) reveals no peculiarities in the value of the effective temperature. However, the value of the surface gravity is an order of magnitude larger for EG 37 and 38 than the average value for the other DAs in the sample. Keeping in mind that gravities have been derived here by measuring the strength of H_β, one would expect lower gravities if the spectrum of both stars were contaminated by a late type companion. Therefore, these two white dwarfs actually have larger gravities or the model atmospheres used to match the strength of H_β are inadequate in these two cases only. It is difficult to judge the possibilities of the two alternatives.

Adopting the first alternative it is necessary to search for errors in another term. Then the next step is to search for an error in the value of the bolometric magnitude. A systematic error in the bolometric correction appears unlikely because the error is not present in other DAs of similar effective temperature. In particular the error is not detected in the hotter DA white dwarfs known as EG 42 (see Figure 9). This conclusion leads to a search for systematic error in the absolute magnitude. A systematic error in the absolute magnitude of EG 37 and 38 implies that their distance is different from the distance of the Hyades cluster.

Strittmatter (1977) suggested to search for a systematic error in the distance by assuring that EG 37 and 38 are members of the carbon mass-radius relation that should lie slightly above the magnesium mass-radius curve in Figure 11. Under this assumption the position of both stars, near the hydrogen mass-radius relation, is due to an erroneous value of the bolometric magnitude. An increase of one unit in the bolometric magnitude corresponds to a change of -0.2 in $\log(R/R_\odot)$ and -0.4 in $\log(M/M_\odot)$. Combination of both changes results in a shift almost transversal to the mass-radius relations presented in Figure 11. Accordingly, if EG 37 and 38 actually populate the carbon mass-radius relation, their

bolometric magnitude is about 1.3 mag fainter than the value derived with the Hyades distance. This is equivalent to a parallax of π = 0."039 for both stars instead of π = 0."022 adopted for the Hyades cluster. The corresponding values of $\log(M/M_{\odot})$ are 0.14 $\pm$ 0.22 for EG 37 and 0.30 $\pm$ 0.22 for EG 38. These new values lend support to the degenerate-dwarf character of both stars.

It is interesting to consider the effect of fainter bolometric magnitudes for EG 37 and 38 upon the two sequences of DA white dwarfs in the H-R diagram (Figure 10). As long as EG 37 and 38 are assumed to be at the distance of the Hyades cluster their bolometric magnitudes fit the brighter sequence. However, if their bolometric magnitudes are fainter by 1.3 mag, as suggested above, both stars become members of the fainter sequence. The shift from the brighter to the fainter sequence results from the fact that the separation of the two sequences is about 1.2 mag. Since the fainter sequence appears to be the crystallization sequence of degenerate dwarfs with mostly carbon in their internal composition it can be seen that these considerations produce a highly consistent scenario for these two white dwarfs. The only requirement is that both stars are foreground to the Hyades cluster. Determination of the trigonometric

parallax of EG 37 and 38 will provide a conclusive test
to the foregoing assumptions.

Eggen and Greenstein (1965a) reported that EG 38
is probably an unresolved double of DA and dMe types.
Also van Altena (1969) has noted that a dM star with
V = 15.04 mag and (B-V) = 1.6 mag plus a DA white dwarf
with V = 14.24 mag and (B-V) = 0.0 satisfy the observed
broad band colors of EG 38 and, at the same time, the
color-magnitude diagram for the Hyades stars. However,
this possibility reduces the bolometric magnitude of the
white dwarf by only 0.3 mag and maintains an uncomfort-
ably large value for the mass. Furthermore, it appears
that the intrinsic brightness of the late type companion
has been exaggerated in order to fit the UBV observations.
The effects of a dM companion are not detected in the
intermediate band colors observed by Graham (1972) or
the colors determined with the u, s, β and y spectral
bands.

In conclusion, the results of the present work
uphold the two sequences of white dwarfs in the H-R dia-
gram and indicate that is rather too early to deny the
existence of crystallization sequences. Further observa-
tions of newly discovered DAs and observations of the
trigonometric parallax of some individual cases may con-
firm the existence of a crystallization sequence formed

by degenerate dwarfs with internal composition of carbon and oxygen.

The following is a note added in proof. The fifth catalogue of trigonometric parallaxes from the Naval Observatory (Harrington et al. 1978) reports a new and more accurate parallax for EG 11 (= L 870-2) that makes the star intrinsically fainter. According to this new value π_{abs} = 0."083 $\pm$ 0."003 in the absolute scale, instead of π_{abs} = 0."064 $\pm$ 0."013 as determined at the Cape Observatory. Consequently, the actual bolometric magnitude of EG 11 is M_{bol} = 12.04 and closer to the fainter sequence in the H-R diagram. Also this result shifts the star from the hydrogen mass-radius relation (see Figure 11) to a position at $\log(R/R_{o})$ = -1.74 $\pm$ 0.10 and $\log(M/M_{o})$ = 0.07 $\pm$ 0.28. The new position is closer to the mass-radius relation for carbon white dwarfs.

APPENDIX A

SPECTRAL RESPONSIVITIES

Table 15 presents the spectral responsivities
of the four spectral bands used in the photometric ob-
servations of this investigation.

The steps taken to derive the different factors
of the individual responsivities have been described in
the last section of Chapter 2.

The spectral responsivity is the product of three
factors: (1) the two mirrors reflectance, (2) the
photomultiplier response, and (3) the filter transmittance.
The filter transmittance is not listed because it can
be derived from the data given for each band.

Table 15. The u, s, β, and y spectral responsivities.

λ nm	Two Mirrors Reflectance %	Photomultiplier Responsivity %	Spectral Band Responsivity %
The u Band			
318	76	43	1
320	76	50	2
322	76	53	4
324	76	56	7
326	76	68	9
328	76	61	12
330	76	64	15
332	76	67	18
334	76	70	20
336	76	72	22
338	76	75	24
340	76	78	25
342	76	80	26
344	76	82	27
346	76	83	28
348	76	85	28
350	76	86	28
352	76	87	27
354	76	88	26
356	76	89	25
358	76	90	24
360	76	91	22
362	76	92	20
364	76	93	16
366	76	94	14
368	76	94	11
370	76	95	8
372	76	96	5
374	76	96	3
376	76	97	1

Table 15. -- <u>Continued</u>, spectral responsivities.

λ nm	Two Mirrors Reflectance %	Photomultiplier Responsivity %	Spectral Band Responsivity %
The s Band			
446	76	95	1
448	76	94	5
450	76	94	12
452	76	93	27
454	76	92	36
456	76	91	40
458	76	90	42
460	76	89	43
462	76	88	42
464	76	87	38
466	76	87	32
468	76	86	24
470	76	85	14
472	76	84	6
474	76	83	2
476	76	82	1

Table 15. -- Continued, spectral responsivities.

λ nm	Two Mirrors Reflectance %	Photomultiplier Responsivity %	Spectral Band Responsivity %
The β Band			
456	76	91	1
458	76	90	2
460	76	89	2
462	76	88	4
464	76	87	6
466	76	87	10
468	76	86	14
470	76	85	21
472	76	84	29
474	76	83	35
476	76	82	39
478	76	8o	40
480	76	80	40
482	76	79	39
484	76	78	39
486	76	76	38
488	76	75	37
490	76	74	36
492	76	72	35
496	76	70	34
498	76	69	32
500	76	68	29
502	76	67	23
504	76	65	18
506	76	64	12
508	76	62	8
510	76	61	5
512	76	60	3
514	76	59	2

Table 15. -- <u>Continued</u>, spectral responsivities.

λ nm	Two Mirrors Reflectance %	Photomultiplier Responsivity %	Spectral Band Responsivity %
<u>The y Band</u>			
516	76	57	2
518	76	56	1
524	76	53	1
526	76	51	1
528	76	50	2
530	76	49	3
532	75	48	4
534	75	47	6
536	75	46	9
538	75	45	13
540	75	44	18
542	75	43	22
544	75	42	24
546	75	41	26
548	75	40	26
550	75	39	25
552	75	38	25
554	74	37	23
556	75	37	28
558	75	36	19
560	75	35	13
562	75	34	10
564	75	34	7
566	75	33	5
568	75	33	3
570	75	32	2
572	75	31	2
574	75	30	1
576	75	30	1

APPENDIX B

VISUAL MAGNITUDES COMPILATION

Table 16 presents the apparent visual magnitude and the number of observations obtained by four different observing groups for a sample of DA white dwarfs. For each entry the weighted average is presented in the last column. These data have been used to derive the mean external error of the V magnitude for the observations of this investigation, as explained in the last section of Chapter 3.

Table 16. Visual magnitudes of selected DA white dwarfs.

EG No.	Eggen and Greenstein m		Graham m		Naval Observatory m		This Work m		Average m	
10	14.10	1	--		--		14.17	1	14.14	2
11	12.84	4	12.79	2	--		12.86	5	12.84	11
15	13.22	2	--		13.22	4	13.21	3	13.22	9
17	13.68	6	--		--		13.59	1	13.68	7
26	14.47	4	14.47	2	--		14.46	3	14.47	9
28	13.80	3	13.80	3	13.81	5	13.74	4	13.79	15
29	15.35	1	--		--		15.24	2	15.28	3
30	14.14	1	14.15	2	--		14.11	1	14.14	4
33	9.52	2	9.52	4	--		9.42	5	9.47	11
34	15.63	3	--		15.59	5	15.65	1	15.61	9
36	14.29	4	14.27	2	--		14.26	2	14.28	8
37	14.02	4	14.05	2	--		13.99	2	14.02	8
38	13.95	4	13.90	2	--		13.78	1	13.91	7
39	13.18	4	14.11	2	--		14.14	1	14.15	7
42	13.82	4	13.86	2	--		13.82	2	13.83	8
46	13.40	1	--		--		13.49	3	13.47	4
50	12.10	2	12.05	4	12.05	4	11.86	4	12.00	14
67	13.32	4	13.29	3	13.31	8	13.29	6	13.30	21
70	12.97	2	13.00	2	--		13.01	1	12.99	5
76	12.90	3	13.09	2	--		13.06	4	13.01	9

Table 16. -- <u>Continued</u>.

EG No.	Eggen and Greenstein m		Graham m		Naval Observatory m		This Work m		Average m	
83	13.60	3	13.70	2	13.65	4	13.68	4	13.65	13
87	13.34	2	13.29	3	--		13.25	4	13.28	9
99	12.30	3	12.34	4	12.31	5	12.33	6	12.32	18
102	12.79	4	12.80	2	--		12.81	6	12.80	12
115	14.36	1	14.33	2	--		14.38	5	14.36	8
123	14.26	5	14.33	2	--		14.36	3	14.30	10
125	13.90	2	--		13.92	2	13.94	1	13.92	5
130	14.00	2	14.05	3	--		14.11	2	14.05	7
131	14.24	4	12.30	2	12.28	3	12.28	2	12.27	11
135	13.69	2	13.66	2	13.71	3	13.62	3	13.67	10
139	11.54	5	11.54	2	11.51	3	11.55	5	11.54	15
150	12.77	2	--		12.73	3	12.84	5	12.79	10
155	12.35	2	--		--		14.34	4	14.34	6
159	13.10	2	--		--		12.97	3	13.02	5
161	15.25	1	--		15.33	5	15.32	1	15.32	7
162	12.90	3	12.96	4	12.93	4	12.94	2	12.93	13
168	14.50	1	--		14.51	6	14.47	3	14.50	10
184	12.50	2	12.46	4	--		12.51	4	12.49	10
199	14.51	2	14.36	3	14.29	2	14.28	2	14.36	9
201	13.01	1	--		--		12.97	4	12.98	5
203	13.82	1	--		--		13.79	2	13.80	3
232	--		--		13.68	3	13.67	2	13.68	5
247	11.80	1	--		11.78	2	11.75	2	11.77	5
261	--		--		12.93	3	13.10	1	12.97	4

APPENDIX C

STROMGREN COLORS

Table 17 lists the (u-b) and (b-y) colors for the 18 white dwarfs with accurate absolute magnitude used by Graham (1972) to plot the M_v versus (b-y) diagram. Figure 12 presents the variation of the absolute magnitude with respect to both colors.

Table 17. Reproduction of Graham's data.

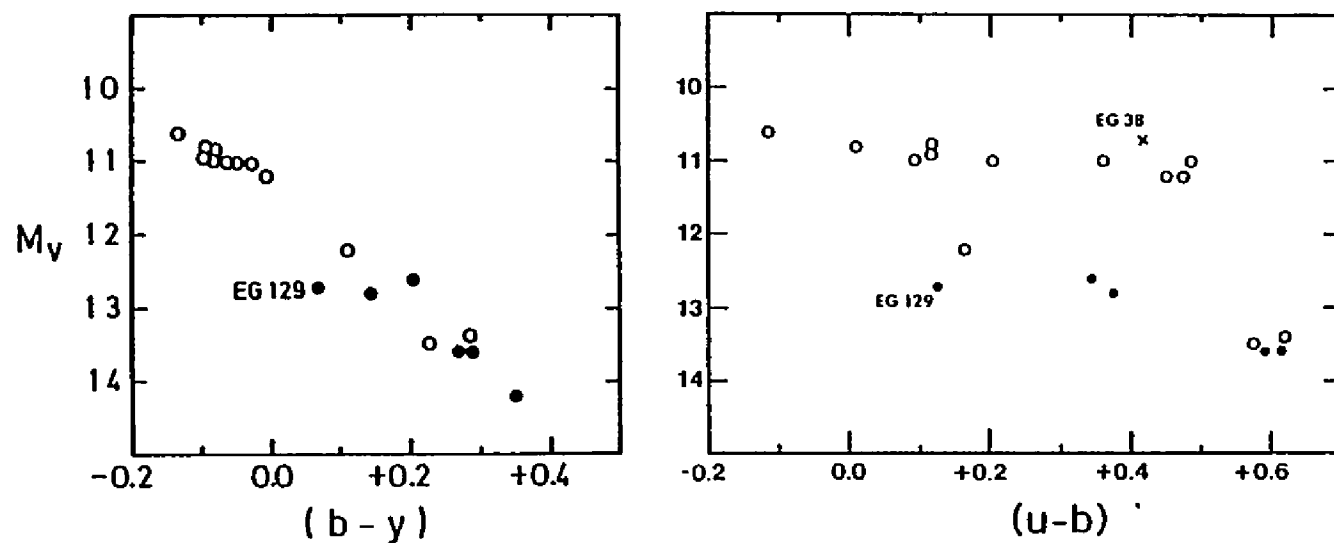| EG No.	(u-b)	M_V	(b-y)
Brighter Sequence			
42	-0.111	10.6	-0.116
37	+0.011	10.8	-0.096
50	+0.092	11.0	-0.089
39	+0.117	10.9	-0.097
139	+0.119	10.8	-0.081
36	+0.201	11.0	-0.058
33	+0.360	11.0	-0.047
38	+0.411	10.7	+0.220
26	+0.471	11.2	-0.005
99	+0.489	11.0	-0.031
Fainter Sequence			
129*	0.124	12.7	+0.073
131	0.166	12.2	+0.113
148*	0.343	12.6	+0.206
119*	0.373	12.8	+0.141
135	0.575	13.5	+0.225
180*	0.590	13.6	+0.269
79*	0.614	13.6	+0.287
199	0.620	13.4	+0.288

* Non-DA white dwarfs.

Figure 12. Absolute magnitude versus Stromgren colors. — The left panel presents the M_V versus (b–y) diagram reproduced from Graham (1972); the right panel variation of M_V with respect to the (u–b) color is presented. Note the separation of about one and one-half magnitude between both sequences. DAs are presented with a circle. A dot is used for other types of white dwarfs.

REFERENCES

Beardsley, W. R., N. E. Wagman, E. Erskine, E. Hubbell and G. Gatewood. 1973. A.J. 78, 95.

Beaver, E. A. and C. E. McIlwain. 1971. Rev. Sci. Instr. 42, 1321.

Bessell, M. S. and D. T. Wickramasinghe. 1978. M.N.R.A.S. 182, 275.

Cameron, A. G. W. 1973. Space Sci. Rev. 15, 121.

Carswell, R. F., P. A. Strittmatter, R. E. Williams, E. A. Beaver and R. Harms. 1975. Ap. J. 195, 269.

Chandrasekhar, S. 1939. Introduction to Stellar Structure. Chicago: University of Chicago Press, p. 412.

Crawford, D. L. and J. V. Barnes. 1970. A.J. 75, 978.

Dahn, Conard C. 1976. Staff member, Naval Observatory, Flagstaff station, Arizona, personal communication.

D'Antona, F. and I. Mazzitelli. 1975. A. and Ap. 44, 253.

Eggen, O. J. 1969. Ap. J. 157, 287.

Eggen, O. and J. L. Greenstein. 1965a. Ap. J. 141, 83.

Eggen, O. and J. L. Greenstein. 1965b. Ap. J. 142, 925.

Eggen, O. and J. L. Greenstein. 1967. Ap. J. 150, 943.

Fontaine, G. and H. M. Van Horn. 1967. Ap. J. Suppl. 31, 467.

Fowler, R. H. 1926. M.N.R.A.S. 87, 114.

Graham, J. A. 1972. A. J. 77, 144.

Greenstein, J. L. 1969. Ap. J. 158, 281.

Greenstein, J. L.   1970.   Ap. J. Letters 162, L55.

Greenstein, J. L.   1974a.   Ap. J. Letters 189, L131.

Greenstein, J. L.   1974b.   Ap. J. Letters 194, L51.

Greenstein, J. L.   1975.   Ap. J. Letters 196, L117.

Greenstein, J. L., J. E. Gunn and J. Kristian.   1971.
    Ap. J. Letters 169, L63.

Hamada, T. and E. E. Salpeter.   1961.   Ap. J. 184, 683.

Hanson, R. B.   1975.   A. J. 80, 379.

Harrington, R. S., C. C. Dahn, A. L. Behall, J. B. Priser,
    J. W. Christy, B. Y. Diepe, H. D. Ables, H. H. Guetter,
    A. V. Hewitt and R. L. Walker.   1975.   Publ. U.S.N.O.,
    2d Ser. XXIV, Part I.

Harrington, R. S., C. C. Dahn, M. Miranian, B. Y. Diepe,
    J. W. Christy, H. H. Guetter, H. D. Ables, A. V.
    Hewitt, F. J. Vrba and R. L. Walker.   1978.   Naval
    Obs. preprint.

Hass, G. and J. E. Waylonis.   1961.   J. Opt. Soc. Am.
    51, 719.

Hayes, D. S. and D. W. Latham.   1975.   Ap. J. 197, 593.

Heintz, W. D.   1973.   A. J. 78, 780.

Holtsmark, J.   1931.   Ann. d. Phys. 9, 338.

IBM.   1974.   Scientific Subroutine Package (IBM/360),
    p. 291.

Jenkins, L. F.   1952.   General Catalogue of Trigonometric
    Stellar Parallaxes (Yale University Obs., New Haven),
    p. 1.

Jenkins, L. F.   1963.   Supplement to the General Catalogue
    of Trigonometric Stellar Parallaxes (Yale University
    Obs., New Haven), p. 1.

Kelley, G. G. 1964. Methods of Experimental Physics: Vol. 2, Electronic Methods. ed. L. Morton (Academic Press, New York), p. 519.

Klemola, A. R., E. A. Harlan, B. McNamara and C. A. Wirtanen. 1975. A. J. 80, 642.

Kurucz, R. L. 1970. S.A.O. Special Report, No. 309, p. 16.

Lamb, D. Q. and H. M. Van Horn. 1975. Ap. J. 200, 306.

Landstreet, J. D. and J. R. P. Angel. 1975. Ap. J. 196, 819.

Liebert, J. 1976. Res. Assoc., Stewart OBS, Private Com.

Liebert, J. J. R. P. Dugel and J. D. Landstreet. 1975. Ap. J. Letters, 202, L139.

Lippincott, S. L. 1973. A. J. 78, 426.

Luyten, W. J. 1945. Ap. J. 101, 131.

Luyten, W. J. 1963. Adv. A. and Ap. 2, 199.

McCook, G. P. and E. M. Sion. 1977. Villanova Univ. Obs. Contr. No. 2.

Mestel, L. and M. A. Ruderman. 1967. M.N.R.A.S. 136, 27.

Mihalas, D. 1975. Multicolor Photometry and the Theoretical H-R Diagram. Edited by A. G. D. Philip and D. S. Hayes, Dudley Obs. Report No. 9, p. 241.

Moore, C. H. 1974. A. and Ap. Suppl. 15, 497.

Nandy, K. 1968. Pub. R. Obs. Edinburg 6, No. 7, 169.

O'Dell, C. R. 1974. I.A.U. Symp. No. 66, Late Stages of Stellar Evolution, edited by R. J. Tayler (Dordrecht-Holland), p. 213.

Oke, J. B. 1974. Ap. J. Suppl. 27, 21.

Oke, J. B. and R. E. Schild. 1970. Ap. J. 161, 1015.

Ostriker, J. P. 1971. Ann. Rev. A. and Ap. 9, 353.

Penston, M. J., M. V. Penston and A. Sandage. 1971.
    Pub. A.S.P. 83, 783.

Peterson, B. A. 1970. A. J. 75, 695.

Philip, A. G. D. and K. D. Philip. 1973. Ap. J. 179,
    855.

Priser, J. B. 1974. Pub. U.S.N.O., Second Series 20,
    Part VII.

Riddle, R. K. 1970. Publ. U.S.N.O., 2nd Ser. XX,
    Part IIIA.

Robben, F. 1971. App. Optics 10, 776.

Routly, P. M. 1972. Publ. U.S.N.O., 2nd Ser. XX,
    Part VI.

Salpeter, E. E. 1961. Ap. J. 134, 669.

Schatzmann, E. 1958. White Dwarfs. (Amsterdam: North-
    Holland), p. 1.

Schulte, D. H. and D. L. Crawford. 1961. Cont. Kitt
    Peak Nat. Obs. No. 10.

Serkowski, K. 1974. Assoc. Prof., Univ. of AZ, Private Com.

Shipman, H. L. 1972. Ap. J. 177, 723.

Sion, E. M. and J. Liebert. 1977. Ap. J. 213, 468.

Spinrad, H., H. E. Smith and D. J. Taylor. 1972.
    Ap. J. 175, 649.

Stock, J. 1969. Vistas in Ast. 11, 127.

Strittmatter, P. A. 1977. Private communication.

Strittmatter, P. A. and D. T. Wickramasinghe. 1971.
    M.N.R.A.S. 152, 47.

Stromgren, B. 1972. Q.J.R.A.S. 13, 153.

Stultz, David. 1974. Staff member, Kitt Peak Obs.,
    Private communication.

Terashita, Y. and S. Matsushima. 1966. Ap. J. Suppl.
    13, 471.

Terashita, Y. and S. Matsushima. 1969. Ap. J. 156, 203.

Thomas, D. V. 1973. M.N.R.A.S. 161, 335.

Turon, P. and M. O. Mennessier. 1975. A. and Ap. 44, 209.

Unsold, A. 1955. Physik der Sternatmospharen, 2nd ed. (Springer-Verlag, Berlin), p. 206.

Upgren, A. R. 1974. A. J. 79, 651.

van Altena, W. F. 1969. A. J. 74, 2.

van Altena, W. F. 1971a. Ap. J. 165, L77.

van Altena, W. F. 1971b. A. J. 76, 932.

van Altena, W. F. 1974. A. J. 79, 826.

Van Horn, H. M. 1968. Ap. J. 151, 227.

Van Horn, H. M. 1970. Ap. J. 160, L53.

Van Horn, H. M. 1977. Prof., Rochester Univ., Priv. Com.

Wagman, N. E. 1967. A. J. 72, 957.

Wehrse, R. 1975. A. and Ap. 39, 169.

Wehrse, R. 1976. A. and Ap. Suppl. 24, 95.

Weidemann, V. 1963. Zs. f. Ap. 57, 87.

Weidemann, V. 1966. J. Quant. Spectr. Rad. Transfer 6, 691.

Weidemann, V. 1971. IAU Symp. No. 42, White Dwarfs, edited by W. J. Luyten, Reidel, Dordrecht, p. 81.

Weidemann, V. 1975. Problems in Stellar Atmospheres and Envelopes. Edited by B. Baschek, W. H. Kegel and G. Trairing (Heidelber: Springer-Verlag), p. 173.

Weidemann, V. 1977. A. and Ap. 59, 411.

Wickramasinghe, D. T. 1972. Mem. R.A.S. 76, 129.

Wickramasinghe, D. T. and P. A. Strittmatter. 1970.
  M.N.R.A.S. <u>150</u>, 435.

Wickramasinghe, D. T. and P. A. Strittmatter. 1972.
  M.N.R.A.S. <u>160</u>, 421.

Wickramasinghe, D. T. and J. Whelan. 1977. M.N.R.A.S.
  <u>178</u>, 11P.

Wickramasinghe, D. T., R. I. Thompson and P. A.
  Strittmatter. 1972. Ap. J. <u>178</u>, 763.

Wildt, R. 1939. Ap. J. <u>90</u>, 611.

Young, T. 1963. App. Optics <u>2</u>, 51.

Young, T. 1969. App. Optics, <u>8</u>, 2431.

Young, T. 1974. <u>Methods of Experimental Physics,
  Vol. 12, Astrophysics, Part A: Optical and Infrared</u>.
  Edited by N. P. Carleton (Academic Press, New York),
  p. 1.